www.sciencemag.org/cgi/content/full/1152677/DC1

Supporting Online Material for

A Model for Neuronal Competition During Development

Christopher D. Deppmann, Stefan Mihalas, Nikhil Sharma, Bonnie E. Lonze, Ernst Niebur, David D. Ginty*

*To whom correspondence should be addressed. E-mail: dginty@jhmi.edu

Published 6 March 2008 on *Science* Express
DOI: 10.1126/science.1152677

This PDF file includes

Other Supporting Online Material for this manuscript includes the following:
(available at www.sciencemag.org/cgi/content/full/1152677/DC1)

Table S2. Microarray data, available as a separate Excel file.

Materials and Methods

Mouse husbandry and genotyping

p75$^{-/-}$ mice (targeted deletion of exon III) (*1*) were generated as described (*2*). NGF$^{+/-}$ mice (*3*) and Bax$^{+/-}$ mice (*4*) were maintained on the C57BL/6 background. The genotyping of these alleles as well as the generation of NGF$^{-/-}$/Bax$^{-/-}$ animals was performed as described previously (*5*).

Microarray analysis

SCGs were removed from P0 pups displaying the Bax null phenotype and were stored individually in RNAlater (Ambion) at -20C awaiting results from both Bax and NGF genotyping. Only the ganglia from *NGF-/-;Bax-/-* or *NGF+/+* were kept for RNA isolation. Ganglia from like genotypes were pooled, and once a minimum of six total ganglia per genotype was collected, RNA was isolated using the RNeasy kit (Qiagen) which yielded 500-1000ng of material. Probe preparation and hybridization to mouse genome chips (Mouse expression set 430, Affymetrix) were carried out by the JHMI Microarray core facility according to standard Affymetrix protocols. Examples of this preparation have been described extensively elsewhere (*6*). Quality of the microarray experiments were assessed using two Bioconductor packages for statistical analysis, affyPLM and Affy. To estimate the gene expression signals, data analysis was conducted on the chips' CEL file probe signal values at the Affymetrix probe pair (perfect match (PM) probe and mismatch (MM) probe) level, using the statistical technique GCRMA (Robust Multi-array Analysis Using GC content for Background adjustment) (*7, 8*) with the bioconductor package gcrma. This probe level data processing includes a normalization procedure utilizing a quantile normalization method (*9*) to reduce the obscuring variation between microarrays, which might be introduced during the processes of sample preparation, manufacture, fluorescence labeling, hybridization and/or scanning. With the signal estimates, Principal Component Analysis (PCA) was performed in R to assess sample variability.

With the signal intensities estimated above, an empirical Bayes method with the lognormal modeling, as implemented in the bioconductor package EBarrays, was used to estimate the posterior probabilities of the differential expression of genes between the sample conditions, i.e. control and knockout samples (*10-12*). The criterion of the posterior probability > 0.5, which means the posterior odds favoring change, was used to produce the differentially expressed gene list. All Bioconductor packages are available at http://www.bioconductor.org and all computation was performed under R environment (http://www.r-project.org;(*13*)).

RT-PCR

RNA was extracted from mass sympathetic neuron cultures using Trizol (Invitrogen) as described by the manufacturer. First strand cDNA was synthesized using random hexamers and the SuperScript III system (Invitrogen). Primers that were used for RT-PCR are as follows:

GAPDH:	F- CCCATCACCATCTTCCAGGA,	R- TTGTCATACCAGGAAATGAGC
MAB21L1:	F- GCTGAACGGAATTCTTCTGC,	R- AGGATCTCTCTTGCCAGTCG

HSPA1b:	F-CACCATCACCAACGACAAGG,	R- TGAAGGCATAGGACTCGAGC
HTR3b:	F- CGTCCATGCTGTATTGGATG,	R- AACCGAATCTGTGCGAAGTC
Alpha-synuclein:	F- AAGAGTCTGTTCGCTGGAGC,	R- TAAGCCTCACTGCCAGGATC
ETV1:	F- AAGAGGAGCAGAATGGATGG,	R- TGTGGCTTCTGATCATAGGC
ETV5:	F- GTGCCTCTACAACTATTGTGCC,	R- TCTCTGTTCTGATGGATACTGGC
RASGRP1:	F- AAGAACTGTCTGAACACCTCACC,	R- GGCTGAGAACCATCAGTTGTACC
BDNF:	F-TGTGCGGACCCATGGGACTC,	R- GCCATGTCCACTGCAGTCTTTT
P75:	F- ATCTTGGCTGCTGTGGTTG,	R- TGTAGAGGTTGCCATCACCC
AKAP7:	F- AGGATGCTGAACTGGTCAGG,	R- CAGCTCTCACTTCCGGTTG
Netrin-g1:	F- AGTGTCCTCTGTGATGCAGC,	R- AATGTGGAGGGATGTCTTCC
TrkA:	F- ATGCTGCGAGGCCAGCGGCA,	R- CCTGACAGGGTCAAGTCCTG
KLF7:	F- GCAGTCATCTGCACTGTACACG	R- CATCCACGGCTGAGAGAG
NT-4	F-CACTGGCTCTCAGAATGCAA	R- GTAGAGCAGTCGAGCCATCC
Sortilin-1	F- AGACATCCTTGAGCGCAACT	R- GAGGAAGTCCTCCAGGGAAC

Sympathetic Neuron Culture and Survival Assays

Sympathetic neuron cultures and survival assays were performed as described previously (*14*). Briefly, neurons were obtained by enzymatic dissociation of P1 (unless otherwise noted) rat or mouse superior cervical ganglia. These neurons were plated for mass or compartmentalized culture experiments in DMEM supplemented with 10% FBS, penicillin/streptomycin (1U/ml) and 50ng/ml of NGF purified from mouse salivary glands (*15*). After the first DIV, the media was supplemented with 5uM Ara-C for 48 hours to remove glial contamination and the NGF concentration was changed as indicated. For compartmentalized cultures, neurons were given time to project their axons into the outer chamber (5-7 DIV) and indicated treatments were performed for 36 hours. Fluorescent microspheres (Invitrogen/Molecular probes) were added to the outer chamber 24 hours prior to scoring cell survival via Hoechst staining (*14*).

***In situ* hybridization**

Probe preparation and *In situ* hybridization was performed as previously described (*16*). Fresh frozen tissue was cryosectioned at a thickness of 14um. The BDNF probe toward Exon 5 was a generous gift from N. Ramanan. Probes for TrkA and NT4 were amplified from a sympathetic neuron cDNA library and cloned into the pBK-CMV vector (Stratagene). The primers used to clone TrkA and NT-4 were as follows:

TrkA- F- GGCCTCGAGGAATCTGTCCTCCAATGCG
R- GGCTCTAGATGACTTGGACAGAGACCTCG
NT-4 – F- GGCCTCGAGCACTGGCTCTCAGAATGCAA
R- GGCTCTAGAAGGCAACCAGAAACAGCCTA

Immunostaining

Fresh frozen tissue was cryosectioned at a thickness of 12um. Sections were fixed for 15 minutes (4% PFA in 1x PBS), washed, blocked (10% Normal Donkey Serum, 0.2% Triton X in 1x PBS), incubated with primary antibody overnight at 4C (5% Normal Donkey Serum, 0.1% Triton X in 1x PBS), washed, incubated with secondary antibody at room temperature for 90 mins (5% Normal Donkey serum, 0.1% Triton X in 1x PBS), and finally washed and mounted (Fluoramount). Primary antibodies used include TrkA (1:1000, Chemicon), tyrosine hydroxylase (1:500, Chemicon), Tuj1 (1:1000, Covance), and p75 (1:1000, Chemicon), P-c-Jun (1:500 Santa Cruz, Cell Signaling). Immunostaining was visualized by confocal microscopy. Cell area and TrkA intensity

were quantified using imageJ.

Immunoblotting and Antibodies
Sympathetic neurons were cultured as described above, and treated as indicated in the main text (*14*). Neurons were lysed with boiling 1.5X SDS-Laemli buffer. Immunoblot analysis was performed on these extracts using antibodies toward p-TrkA (1:1000, Cell Signaling), p-Akt (1:1000, Cell Signaling), p-MAPK (1:1000, Cell Signaling), Tuj1 (1:5000, Covance), TrkA (1:1000, Chemicon), TH (1:500, Chemicon). Unless otherwise indicated, Tuj1 was used to normalize protein concentration. ImageJ was used to quantify band intensities.

Nissle staining and cell counts
For neuron counts of the SCG, fresh frozen tissue was sectioned at a thickness of 10um and every 5th section was processed for Nissl staining as previously described (*17*). Counting was performed as previously described (*18*).

Statistical analysis
An ANOVA test was performed followed by a Tukey's Post Hoc test for all groups of data. All time points for the $p75^{-/-}$ vs. wild-type SCG counts had an n=3. All conditions for campenot chamber survival experiments had an n>3. All in vitro survival experiments had an n=3.(*2*)

Supplemental Material for the Mathematical Model

Model Equations

A simplified description of TrkA production, activation and signal duration in neurons considers only two states for TrkA: free ($TrkAf$) and NGF-bound, or activated ($TrkAa$). TrkA is synthesized in the free or inactive form, is activated upon NGF binding, and degraded in both the active and inactive forms, which affects signal duration.

$$\begin{aligned} TrkAf_i'(t) &= Vsyn_i(t) - kon \times NGF(t) \times TrkAf_i(t) + koff \times TrkAa_i(t) - Vdepf_i(t) \times TrkAf_i(t) \\ TrkAa_i'(t) &= kon \times NGF(t) \times TrkAf_i(t) - koff \times TrkAa_i(t) - Vdepa_i(t) \times TrkAa_i(t) \\ NGF'(t) &= pr - V_{depNGF} \times NGF(t) - volR \times \sum_i \left(kon \times NGF(t) \times TrkAf_i(t) - koff \times TrkAa_i(t) \right) \end{aligned} \quad (1)$$

where:

- $TrkAf_i$ - concentration of free TrkA in cell i
- $TrkAa_i$ - concentration of active TrkA in cell i
- NGF - concentration of NGF in the extracellular space
- $Vsyn_i(t)$ - rate of TrkA production in cell i
- $Vdepf_i(t)$ - rate constant of free TrkA degradation in cell i
- $Vdepa_i(t)$ - rate constant of active TrkA degradation in cell i
- kon - rate constant of NGF binding to TrkAf
- $koff$ - rate constant of NGF dissociation from TrkAa

- pr - rate of NGF production
- V_{depNGF} - rate constant of NGF depletion
- $volR$ - ratio between the volume of a neuron and the volume of the target tissue

Association and dissociation between NGF and TrkA are much faster processes than TrkA synthesis and degradation which leads to quasistatic equilibrium for free and active TrkA (adiabatic approximation). For each neuron:

$$\begin{aligned} TrkAf_{i,adiab}'(t) = & \quad -kon \times NGF \times TrkAf_{i,adiab}(t) + koff \times TrkAa_{i,adiab}(t) \\ TrkAa_{i,adiab}'(t) = & \quad kon \times NGF \times TrkAf_{i,adiab}(t) - koff \times TrkAa_{i,adiab}(t) \end{aligned} \tag{2}$$

which, as $t \to \infty$, has the solution

$$TrkAa_{i,adiab} = kon/koff \times NGF \times TrkAf_{i,adiab} \tag{3}$$

This corresponds to a state when a quasi static equilibrium is reached, in which the time derivative of any TrkA state is much smaller than the terms corresponding to NGF association or dissociation. At any time, the solution of (1) is a small perturbation from the quasi static equilibrium:

$$TrkAa_i(t) = (1+\alpha_i(t))kon/koff \times NGF(t) \times TrkAf_i(t) \tag{4}$$

where $|\alpha_i(t)| \ll 1$. Thus, $1+\alpha_i(t) \cong 1$. Using equation (4) we express TrkAa and TrkAf in terms of the total TrkA concentrations:

$$\begin{aligned} TrkAf_i(t) &= \frac{TrkA_i(t)}{1+(1+\alpha_i(t))\dfrac{NGF(t)}{Kd}} \\ TrkAa_i(t) &= \frac{TrkA_i(t)}{1+\dfrac{1}{(1+\alpha_i(t))\dfrac{NGF(t)}{Kd}}} \end{aligned} \tag{5}$$

where: $Kd = koff / kon$.

The system of equations (1) becomes:

$$\begin{aligned} TrkA_i'(t) &= Vsyn_i(t) - \frac{Vdepf_i(t)}{1+\dfrac{NGF(t)}{Kd}} \times TrkA_i(t) - \frac{Vdepa_i(t)}{1+\dfrac{Kd}{NGF(t)}} \times TrkA_i(t) \\ NGF'(t) &= pr - V_{depNGF} \times NGF(t) - volR \times \sum_i \left(Vdepa_i(t) \times TrkAa_i(t) \right) - volR \times \sum_i TrkAa_i'(t) \end{aligned} \tag{6}$$

Every term in (6) has an intuitive meaning. The equation for TrkA time derivative consists of a term characterizing synthesis, and two terms characterizing depletion: the

first for depletion of free and the second for depletion of active TrkA. The equation for free NGF time derivative consists of a production term, an NGF depletion term in the target tissue, a term equal to the sum of all TrkA-bound NGF degradation in all neurons and a term equal to the sum of all TrkA-bound NGF accumulations in all neurons.

Using the physiologically realistic approximation that the quantity of NGF in the target tissue is much larger than the quantity of NGF bound to TrkA in all neurons, the last term in equations (6) can be neglected. When integrated this term corresponds to the total TrkA-bound NGF accumulated in neurons. The penultimate term, when integrated, corresponds to the total NGF amount which was degraded inside neurons, and will not be neglected.

$$\begin{aligned} TrkA_i'(t) &= Vsyn_i(t) - TrkA_i(t) \times \left(\frac{Vdepf_i(t)}{1+\frac{NGF(t)}{Kd}} + \frac{Vdepa_i(t)}{1+\frac{Kd}{NGF(t)}} \right) \\ NGF'(t) &= pr - V_{depNGF} \times NGF(t) - \frac{volR}{1+\frac{Kd}{NGF(t)}} \times \sum_i (Vdepa_i(t) \times TrkA_i(t)) \end{aligned} \tag{7}$$

We used equations (7) for most of the simulations.

It is possible to improve the approximation used in equation (7) and estimate the correction term. We used the approximations that $\left|NGF'(t)/NGF(t)\right| \ll \left|TrkAf_i'(t)/TrkAf_i(t)\right|$ and $\left|\alpha_i'(t)\right| \ll \left|TrkAf_i'(t)/TrkAf_i(t)\right|$ only in the correction term, to estimate the effects of active TrkA degradation and accumulation on NGF concentration in the target tissue:

$$\begin{aligned} V_{depNGFTrkAi}(t) &= volR \times \left(\frac{Vdepa_i(t) \times TrkA_i(t)}{1+\frac{Kd}{NGF(t)}} + \frac{TrkA_i'(t)}{1+\frac{Kd}{NGF(t)}} \right) = \\ &= \frac{volR}{1+\frac{Kd}{NGF(t)}} \left(Vsyn_i(t) - TrkA_i(t) \times \left(\frac{Vdepf_i(t)}{1+\frac{NGF(t)}{Kd}} + \frac{Vdepa_i(t)}{1+\frac{Kd}{NGF(t)}} \right) - Vdepa_i(t) \times TrkA_i(t) \right) = \\ &= \frac{volR}{1+\frac{Kd}{NGF(t)}} \times \left(Vsyn_i(t) + \frac{Vdepa_i(t) - Vdepf_i(t)}{1+\frac{NGF(t)}{Kd}} \times TrkA_i(t) \right) \end{aligned} \tag{8}$$

where: $V_{depNGFTrkAi}(t)$ represents the depletion of NGF caused by active TrkA

accumulation and degradation.

Using the result from (8), equation (6) becomes:

$$TrkA_i'(t) = Vsyn_i(t) - TrkA_i(t) \times \left(\frac{Vdepf_i(t)}{1 + \frac{NGF(t)}{Kd}} + \frac{Vdepa_i(t)}{1 + \frac{Kd}{NGF(t)}} \right)$$
$$NGF'(t) = pr - V_{depNGF} \times NGF(t) - \frac{volR}{1 + \frac{Kd}{NGF(t)}} \times \sum_i \left(Vsyn_i + \frac{Vdepa_i(t) - Vdepf_i(t)}{1 + \frac{NGF(t)}{Kd}} \times TrkA_i(t) \right) \quad (9)$$

The simulated differences caused by the correction term in (9) are small as observed in fig. S15.

Basic model

For the basic model we consider the rate of TrkA synthesis and the rate constant of TrkA degradation to be constants.

$$\begin{aligned} Vsyn_i(t) &= Vsyn \\ Vdepa_i(t) &= Vdepa \\ Vdepf_i(t) &= Vdepf \end{aligned} \quad (10)$$

Using (10) in either (4) or (9) leads to the same equilibrium solution. Using this dynamic model the neurons do not compete for NGF, active TrkA rapidly converges to the same equilibrium value for each neuron (Fig. 2A, D-F):

$$TrkA_{equil} = Vsyn \times \frac{Kd + NGF_{equil}}{Vdepf \times Kd + Vdepa \times NGF_{equil}}$$

where the equilibrium value for NGF concentration is:

$$\begin{aligned} NGF_{equil} = \frac{1}{2Kd \times Vdepa \times V_{depNGF}} (& pr \times Vdepa - Kd \times Vdepf \times V_{depNGF} \\ & - N \times volR \times Vdepa \times Vsyn \pm (4 \times Kd \times prod \times Vdepa \times Vdepf \times V_{depNGF} + \\ & (pr \times Vdepa - Kd \times Vdepf \times V_{depNGF} - N \times volR \times Vdepa \times Vsyn)^2)^{\frac{1}{2}}) \end{aligned}$$

In the limit that $VdepNGF$ is 0, the equilibrium NGF concentration is:

$$NGF_{equil} = \frac{Vdepf}{Vdepa} \frac{Kd_{NGF}}{N \times \frac{volR \times Vsyn}{prod} - 1} \tag{11}$$

The solution for TrkA is unique, thus no competition is possible in these conditions. An example of the basic model is presented in Fig 2A and fig. S4A-C. The solution is stable to variations in individual TrkA concentrations: e.g. if TrkA in cell i is higher than the equilibrium value while NGF is at equilibrium, the derivative of TrkA concentration is negative.

Synthesis of TrkA

We observed a positive feedback loop in which NGF activates the expression of it's own receptor, TrkA (Fig 1A-C). If TrkA directly activates its own expression, the production term will depend on the concentration of active TrkA as expressed via a Hill function.

$$Vsyn_i(t) = Vsyn0 + \frac{Vsyn1}{1 + \left(\frac{ksyn}{TrkAa_i(t)} \right)^h} \tag{12}$$

where:

- $Vsyn0$ - rate of TrkA synthesis in the absence of NGF
- $Vsyn1$ - additional rate of TrkA synthesis in the presence of saturating NGF
- $ksyn$ - concentration of active TrkA at which the TrkA-dependent expression is at half-maximal rate
- h - Hill coefficient

Using (12) the system of equations (7) describing N neurons becomes:

$$\begin{aligned} TrkA_i'(t) = \quad & Vsyn0 + \frac{Vsyn1}{1 + \left(\frac{ksyn\left(1 + \frac{Kd}{NGF(t)}\right)}{TrkA_i(t)} \right)^h} - TrkA_i(t) \times \left(\frac{Vdepf_i(t)}{1 + \frac{NGF(t)}{Kd}} + \frac{Vdepa_i(t)}{1 + \frac{Kd}{NGF(t)}} \right) \\ NGF'(t) = \quad & pr - V_{depNGF} \times NGF(t) - \frac{volR}{1 + \frac{Kd}{NGF(t)}} \times \sum_i (Vdepa_i(t) \times TrkA_i(t)) \end{aligned} \tag{13}$$

In order to reduce the number of parameters to be fit we normalized $TrkA$ and NGF to their half-activation values.

$$TrkAn_i'(t) = Vsyn0n + \frac{Vsyn1n}{1+\left(\frac{1+\frac{1}{NGFn(t)}}{\frac{}{TrkAn_i(t)}}\right)^h} - TrkAn_i(t)\times\left(\frac{Vdepf_i(t)}{1+NGFn(t)} + \frac{Vdepa_i(t)}{1+\frac{1}{NGFn(t)}}\right)$$

$$NGFn'(t) = prn - V_{depNGF}\times NGFn(t) - \frac{volRn}{1+\frac{1}{NGFn(t)}}\times\sum_i (Vdepa_i(t)\times TrkAn_i(t)) \quad (14)$$

where:

- $TrkAn_i(t) = TrkA_i(t)/ksyn$
- $Vsyn0n = Vsyn0/ksyn$
- $Vsyn1n = Vsyn1/ksyn$
- $NGFn(t) = NGF(t)/Kd_{NGF}$
- $prn = pr/Kd_{NGF}$
- $volRn = volR\times ktr/Kd_{NGF}$

TrkA expression levels during development are best fit if TrkA expression depends on NGF-bound TrkA concentration via a Hill function with a coefficient 1. When the Hill coefficient h is 1, as obtained from the fit of TrkA mRNA during development (fig. S2), the equation for the equilibrium solution for TrkA is quadratic. It has two solutions: one positive and one negative. The positive solution is stable: if the concentration of TrkA in a cell is slightly higher than the equilibrium, the rate of TrkA production will be smaller than the rate of TrkA depletion and vice-versa. Thus, the positive feedback loop of NGF-bound TrkA controling expression of TrkA is not sufficient to cause competition among neurons. An example showing a set of neurons converging to the same trophic state is presented in Fig 2B and fig. S4D-F.

Modeling the Control of TrkA Degradation

Saturating TrkA degradation

We observed an increase in TrkA signal duration after TrkA activation (Fig 1). We assume this is a result of a decrease in the rate constant of TrkA depletion. One possible way to slow the rate constant of TrkA degradation with increasing TrkA signaling is to consider that the degradation rate saturates. In this case, the equation for the rate constant is:

$$Vdepa_i(t) = \frac{Vdepa1}{1 + \frac{TrkAn_i(t)}{Kd_{dep} \times \left(1 + \frac{1}{NGFn(t)}\right)}}$$
$$Vdepf_i(t) = \frac{Vdepf1}{1 + \frac{TrkAn_i(t)}{Kd_{dep} \times \left(1 + \frac{1}{NGFn(t)}\right)}} \quad (15)$$

where:

- $Vdepa1$ - rate constant of active TrkA degradation for small TrkA concentrations
- $Vdepf1$ - rate constant of free TrkA degradation for small TrkA concentrations
- Kd_{dep} - half-saturation constant

Using (15) in (14) and considering the Hill coefficient h to be 1, the equilibrium equation for TrkA is quadratic:

$$\left(Vsyn0n \times \left(1 + \frac{1}{NGFn} + TrkAn_i\right) + Vsyn1n \times TrkAn_i\right) \times \left(1 + \frac{TrkAn_i}{Kd_{dep}\left(1 + 1/NGFn\right)}\right) =$$
$$= TrkAn_i \left(1 + \frac{1}{NGFn} + TrkAn_i\right) \times \left(\frac{Vdepf1}{1 + NGFn} + \frac{Vdepa1}{1 + 1/NGFn}\right)$$

Consequently, for some NGF concentrations, it is possible to obtain two solutions for $Vsyn(TrkA, NGF) = Vdep(TrkA, NGF) \times TrkA$, when synthesis and degradation of TrkAa are equal, however one of these solutions is unstable. It leads to unlimited accumulation of $TrkA$.

One way to avoid indefinite TrkA accumulation is to consider the saturation of TrkA depletion to be different for free and active TrkA. Another way is to consider two parallel degradation pathways for active TrkA: one with a high rate constant which saturates at higher TrkA concentrations and another with a low rate constant which does not saturate:

$$Vdepa_i(t) = Vdepa0 + \frac{Vdepa1}{1 + \frac{TrkAn_i(t)}{Kd_{dep} \times \left(1 + \frac{1}{NGFn(t)}\right)}}$$
$$Vdepf_i(t) = Vdepf0 \quad (16)$$

where:

- $Vdepa0$ - rate constant of active TrkA degradation for saturating TrkA and NGF
- $Vdepa0 + Vdepa1$ - rate constant of TrkA degradation for low TrkA or NGF concentrations

With the degradation term presented in (16) but considering only the basic model for TrkA synthesis, the equilibrium equation for TrkA is quadratic as well:

$$Vsyn0\times\left(1+\frac{TrkA_i}{Kd_{dep}\left(1+1/NGFn\right)}\right)=$$

$$=TrkA_i\times\frac{Vdepa1}{1+1/NGFn}+TrkA_i\times\left(1+\frac{TrkA_i}{Kd_{dep}\left(1+1/NGFn\right)}\right)\times\left(\frac{Vdepf0}{1+NGFn}+\frac{Vdepa0}{1+1/NGFn}\right)$$

with an example shown in fig. S4G-I.

With the TrkA depletion term specified in (16), equations (14) become:

$$\begin{aligned}TrkAn_i'(t)&=Vsyn0n+\frac{Vsyn1n}{1+\left(\frac{1+\frac{1}{NGFn(t)}}{TrkAn_i(t)}\right)^h}\\&\quad-TrkAn_i(t)\times\left(\frac{Vdepf0}{1+NGFn(t)}+\frac{Vdepa0}{1+\frac{1}{NGFn(t)}}+\frac{Vdepa1}{1+\frac{1}{NGFn(t)}+\frac{TrkAn_i(t)}{Kd_{dep}}}\right)\\NGFn'(t)&=prn-V_{depNGF}\times NGFn(t)-\\&\quad-volRn\times\sum_i\left(\left(\frac{Vdepa0}{1+\frac{1}{NGFn(t)}}+\frac{Vdepa1}{1+\frac{1}{NGFn(t)}+\frac{TrkAn_i(t)}{Kd_{dep}}}\right)\times TrkAn_i(t)\right)\end{aligned}\qquad(17)$$

Including both the degradation term in (16), and the synthesis term in (12) the equilibrium equation for TrkA becomes cubic:

$$\left(Vsyn0\times\left(1+\frac{1}{NGFn}+TrkA_i\right)+Vsyn1\times TrkA_i\right)\times\left(1+\frac{TrkA_i}{Kd_{dep}\left(1+1/NGFn\right)}\right)=$$

$$=TrkA_i\left(1+\frac{1}{NGFn}+TrkA_i\right)\times\frac{Vdepa1}{1+1/NGFn}+$$

$$+TrkA_i\left(1+\frac{1}{NGFn}+TrkA_i\right)\times\left(1+\frac{TrkA_i}{Kd_{dep}\left(1+1/NGFn\right)}\right)\times\left(\frac{Vdepf0}{1+NGFn}+\frac{Vdepa0}{1+1/NGFn}\right)$$

It is thus possible to find NGF concentrations, which allow three stable *TrkA* solutions for low and high trophic signaling states, and an intermediate state that is unstable (fig. S4J). Shown in Fig 2C is an example of neurons competing for NGF which have, after completing the competition process, a bimodal distribution of TrkA, with the modes corresponding to the stable solution.

TrkA Protection from Degradation

Another possible way to slow the rate constant of TrkA degradation with increasing TrkA concentrations is to consider that NGF-TrkA signaling leads to production of a factor which protects TrkA from degradation.

$$Vdepa_i(t) = \frac{Vm}{1+\frac{prmax}{1+\frac{Kdpr\left(1+1/NGFn(t)\right)}{TrkAn_i(t)}}} \tag{18}$$

where

- Vm - rate constant of TrkA degradation for low TrkA concentrations
- $prmax$ - normalized maximal concentration of the protective factor
- $Kdpr$ - half activation value of the protective mechanism

Equations (16) and (18) have the same dependence on $TrkAn_i$ with the equivalence between parameters being given by:

$$\begin{aligned} Vdepa0 &= Vm/(prmax+1) \\ Vdepa1 &= Vm\times prmax/(prmax+1) \\ Kd_{dep} &= Kdpr/(prmax+1) \end{aligned} \tag{19}$$

Apoptotic Signal

We observed that TrkA signaling both increases its own synthesis and prolongs its signal duration (Figure 1). These elements are sufficient to create competition among neurons for NGF and survival leading to a bimodal distribution of trophic signal strength in which neurons with low trophic signal strength die. However, this process is slow and leads to developmental stages which are different from those observed. In the model described so far, the period of exponential increase neuronal trophic signal strength is generally followed by a period of intense competition in which the average trophic signal strength decreases, followed by a period of neuronal death. In the experimental findings the period of exponential increase in trophic signal strength partially superimposes the period of neuronal death. One possible mechanism to expedite the competition is to consider a mechanism in which the neurons with high trophic signal strength contribute to the death of those with low trophic signal strength.

Two apoptotic cues for sympathetic neurons are BDNF and NT-4 (Fig. 3) (*19,20*). BDNF and NT4 apoptotic signals are produced by sympathetic neurons and we assume their production rate is proportional to the trophic signal strength while their depletion is linear with concentration: The BDNF notation in our equations represents all the apoptotic signals.

$$BDNF'(t) = \sum_i \left(\frac{Pr_{BDNF}}{1+\frac{Kd_{PUN}\left(1+1/NGFn(t)\right)}{TrkAn_i(t)}} \right) - V_{BDNF}\times BDNF(t) \tag{20}$$

where:
• $BDNF(t)$ - concentration of the apoptotic signal in the sympathetic ganglion

This equation introduces three new free parameters:
• Pr_{BDNF} - maximal rate of apoptotic signal production by a neuron
• Kd_{PUN} - concentration of active TrkA which leads to half-activation of apoptotic signals production
• V_{BDNF} - rate constant of apoptotic signal depletion.

The apoptotic signals BDNF and NT4 bind to and activate the p75 receptor. We normalize the concentration of the apoptotic signal to its dissociation constant from the p75 receptor.

$$BDNFn'(t) = \sum_i \left(\frac{Pr_{BDNFn}}{1 + \frac{Kd_{PUN}\left(1 + 1/NGFn(t)\right)}{TrkAn_i(t)}} \right) - V_{BDNF} \times BDNFn(t) \qquad (21)$$

where
• $BDNFn(t) = BDNF(t) / Kd_{p75BDNF}$
• $Pr_{BDNFn} = Pr_{BDNF} / Kd_{p75BDNF}$
• $Kd_{p75BDNF}$ - dissociation constant of apoptotic signal from p75

The expression of p75 developmentally follows TrkA expression (*21*), and is, at least in part, NGF-dependent (*22*). Therefore we consider terms for p75 expression to depend on the concentration of active TrkA via a Hill function. The depletion of p75 receptors is considered to occur in both the free and the active states:

$$p75_i'(t) = \frac{Vp75}{1 + \frac{Kd_{p75} \times \left(1 + 1/NGFn(t)\right)}{TrkA_i(t)}} - \left(\frac{Vdepp75f}{1 + BDNFn(t)} + \frac{Vdepp75a}{1 + 1/BDNFn(t)} \right) \times p75_i(t) \qquad (22)$$

where:
• $Vp75$ - maximal rate of p75 expression
• Kd_{p75} - concentration of active TrkA required for half activation of p75 expression
• $Vdepp75f$ - rate constant of free p75 depletion
• $Vdepp75a$ - rate constant of active p75 depletion

The depletion of p75 receptors with apoptotic molecules bound to it results in an additional consumption term for the apoptotic signal:

$$BDNFn'(t) = \sum_i \left(\frac{Pr_{BDNFn}}{1 + \frac{Kd_{PUN}\left(1 + 1/NGFn(t)\right)}{TrkAn_i(t)}} \right) - V_{BDNF} \times BDNFn(t) - \\ - \frac{volRgangn}{1 + 1/BDNFn(t)} \times Vdepp75a \times \sum_i (p75_i(t)) \tag{23}$$

where $volRgang$ is the ratio between the volume of a neuron to that of the sympathetic ganglion divided by the dissociation constant of the apoptotic molecules from p75.

The effect of the apoptotic signal is considered to be strongly nonlinear, in fact binary: if the concentration of active $p75_i$ is below a threshold the apoptotic signal has no effect on the neuron i, while if it is above this threshold, then the apoptotic signal contributes to trophic signal strength depletion.

The influence of protective signals is also considered binary: if the concentration of active $TrkAn_i$ is above a threshold the apoptotic signal has no effect on the neuron i. To model these influences we add a term to the equations for $TrkAn$ dependence on time (17):

$$Ap_i(t) = Ap_k \times TrkAn_i(t) \times \theta\left(TrkA_{tr} \times \theta\left(p75_{tr} - \frac{p75(t)}{1 + 1/BDNFn(t)} \right) - \frac{TrkAn_i(t)}{1 + 1/NGFn(t)} \right) \tag{24}$$

where:

- Ap_k - rate constant of TrkA loss in the neurons affected by the apoptotic signal
- $\theta(x)$ - Heaviside step function: $\theta(x) = 0$ if $x < 0$ and $\theta(x) = 1$ if $x \geq 0$
- $p75_{tr}$ - threshold for active $p75_i$
- $TrkA_{tr}$ - threshold for protection

By adding the term (24) caused by the apoptotic signal to TrkA equations (17), and complementing the system of equations with the time dependence of the apoptotic signal (23) and its receptor (22), the set of equations characterizing the competition with apoptotic signal is:

$$TrkAn_i'(t) = Vsyn0n + \frac{Vsyn1n}{1+\left(\frac{1+\frac{1}{NGFn(t)}}{TrkAn_i(t)}\right)^h} -$$

$$- TrkAn_i(t) \times \left(\frac{Vdepf0}{1+NGFn(t)} + \frac{Vdepa0}{1+\frac{1}{NGFn(t)}} + \frac{Vdepa1}{1+\frac{1}{NGFn(t)}+\frac{TrkAn_i(t)}{Kd_{dep}}} \right) +$$

$$- Ap_k \times TrkAn_i(t) \times \theta\left(TrkA_{tr} \times \theta\left(p75_{tr} - \frac{p75(t)}{1+1/BDNFn(t)} \right) - \frac{TrkAn_i(t)}{1+1/NGFn(t)} \right)$$

$$NGFn'(t) = prn - V_{depNGF} \times NGFn(t) -$$

$$- volRn \times \sum_i \left(\left(\frac{Vdepa0}{1+\frac{1}{NGFn(t)}} + \frac{Vdepa1}{1+\frac{1}{NGFn(t)}+\frac{TrkAn_i(t)}{Kd_{dep}}} \right) \times TrkAn_i(t) \right)$$

$$p75_i'(t) = \frac{Vp75}{1+\frac{Kd_{p75} \times (1+1/NGFn(t))}{TrkA_i(t)}} - \left(\frac{Vdepp75f}{1+BDNFn(t)} - \frac{Vdepp75a}{1+1/BDNFn(t)} \right) \times p75_i(t)$$

$$BDNFn'(t) = \sum_i \left(\frac{Pr_{BDNFn}}{1+\frac{Kd_{PUN}(1+1/NGFn(t))}{TrkAn_i(t)}} \right) - V_{BDNF} \times BDNFn(t) -$$

$$- \frac{volRgangn}{1+1/BDNFn(t)} \times Vdepp75a \times \sum_i (p75_i(t)) \qquad (25)$$

An example simulation using the model with apoptotic signal is shown in Fig 4 and figs. S10 – S16.

Parameter Values

Initial concentrations

The final surviving neurons have a TrkA concentration close to the half activation value, and roughly 50% of the neurons survive, corresponding to an average *TrkAn* of 0.5. Measurement of TrkA levels following NGF treatment show a maximal change of a factor of approximately 10. Therefore the initial distribution chosen for *TrkAn* has a mean of 0.05. We chose the initial distribution to be normal and with a standard deviation ten times smaller than the mean. Varying the initial distribution does not lead to large variations in the final neuron number (fig. S5), however to reproduce the developmental stage in which average *TrkAn* has an exponential growth it needs to start

at values $\ll 1$. The time 0 of the simulation corresponds to embryonal day E15, when axons of many SCG neurons arrive at their target.

Assuming that the concentration of NGF in the target tissue is of the same order of magnitude as its affinity for TrkA, and that before innervation its concentration is higher than the average, we considered [NGF] to be 2 times higher than its affinity for TrkA. Varying starting [NGF] does not lead to large variations in the final neuron number (fig. S5).

The initial apoptotic signal concentration and p75 concentration are assumed to be zero.

Reducing the initial number of neurons results naturally in an increased number of neurons surviving, and surprisingly an increased competition time (fig. S6).

Regulation of TrkA Expression

In the period immediately following the arrival of the axons of sympathetic neurons at their final target, TrkA expresion levels are low and there is little competition for NGF. In the limit $TrkAn_i(t) \ll 1$, $NGFn(t) \gg 1$ and $Vsyn0n \ll Vsyn1n \times TrkAan_i(t)^h$ and neglecting TrkA degradation, equations (17) reduce to:

$$TrkA_i'(t) = Vsyn1n \times TrkA_i(t)^h \tag{26}$$

If $h = 1$, then equation (26) leads to $TrkA_i(t) = \exp(Vsyn1n \times (t - t_0))$ where t_0 is an integration constant. The concentration of TrkA mRNA during the development of the mouse SCG has been measured previously. Using values for the time dependence of TrkA mRNA concentrations at E13-E19 (*21*) gives a relationship that is remarkably well fit by an exponential: $R^2 = 0.985$ in a linear regression of the logarithm of TrkA mRNA concentration. Performing a nonlinear regression with an exponential model, the unexplained variance divided by the data variance is 1.7×10^{-3}. If $h \neq 1$, then equation (26) leads to $TrkA_i(t) = (Vsyn1n \times (h-1) \times t_0 - t))^{-1/(h-1)}$. The Levenberg Marquardt method for nonlinear regression does not converge when using the model for $h \neq 1$. If we force $h = 2$ and perform a nonlinear regression, the unexplained variance divided by the data variance is 5.4×10^{-2}, more than two orders of magnitude higher than for $h = 1$, as can be observed in fig. S2. We conclude that the observed exponential rise in TrkA expression levels is best fit by $h = 1$.

However, using $h = 1$, there is only one stable solution for $TrkAn_i$ which leads to the same final concentration for TrkA in all neurons, inconsistent with the experimental evidence showing a bimodal TrkA expression pattern (Fig 1). Multiple stable solutions are possible if $h > 1$. If $h >> 1$, the time dependence of TrkA concentration during early development deviates drastically from the observed exponential growth. If $h = 1 + \alpha, \alpha << 1$, the multiple stable solutions for $TrkAn_i$ are obtained only for a narrow range of NGF concentrations. One possibility to obtain bistability while keeping $h = 1$ is to consider that TrkA activation slows down the rate of TrkA degradation.

Using $h = 1$, it is possible to obtain a solution even when relaxing some of the constraints used, which leads to a better fit of the model parameters. If we relax the

constraint that $TrkAn_i(t) \ll 1$, equation reduces to:

$$TrkA_i'(t) = \frac{Vsyn1}{1 + \frac{ksyn}{TrkA_i(t)}} \tag{27}$$

These have the solutions:

$$TrkA_i(t) = ksyn \times W\left(\frac{\exp((t - t0) \times Vsyn1/ksyn)}{ksyn}\right) \tag{28}$$

where W is the Lambert product log function. Performing a nonlinear regression of the time dependence of TrkA mRNA concentration using the model given by (28) allows us to estimate ksyn. The best fit functions are presented in fig. S2. The value of ksyn is used to normalize the data to perform an additional regression.

If we relax the constraint that $Vsyn0n << 1$, consider that NGF concentration is close to its affinity for TrkA: $NGFn(t) \cong 1$ and assume $Kddep << 1$, equations (17) reduce to:

$$TrkAn_i'(t) = Vsyn0n - Vdepa1 \times Kddep + (Vsyn1n - Vdepa0 - Vdepf0)/2 \times TrkAn_i(t) \tag{29}$$

These have the solutions:

$$TrkAn_i(t) = -2\frac{Vsyn0n - Vdepa1 \times Kddep}{Vsyn1n - Vdepa0 - Vdepf0} + exp((Vsyn1n - Vdepa0 - Vdepf0)/2 \times (t - t0)) \tag{30}$$

Using (30) as the model for a nonlinear regression of the normalized data set, the best fit value for $Vsyn0n - Vdepa1 \times Kddep$ is $4.35 \times 10^{-3}\, days^{-1}$ with a 95% confidence interval $(-4.12, 12.8) \times 10^{-3}\, days^{-1}$. $Vsyn1n - Vdepa0 - Vdepf0$ is $1.424\, days^{-1}$ with a 95% confidence interval $\{1.26, 1.59\}\, days^{-1}$. We interpret the first fit as a constraint $Vsyn0n - Vdepa1 \times Kddep \ll 1 day^{-1}$. We selected the values $Vsyn1n = 4 days^{-1}$ and $Vdepa0 = 2 days^{-1}$. The difference between these parameters has a large impact on competition (figs. S8, S9).

Degradation of TrkA

From Fig 1D, the order of magnitude for Vdepa0 is 1/day. Simulations of the equilibrium TrkA concentration as a function of NGF concentration show a biphasic response (fig. S3A). The ratio of the peak value to the value in saturating NGF is mainly dependent on Vsyn1n, Vdepa0 and Vdepf0. The values used previously (ie $Vsyn1n = 4 days^{-1}$ and $Vdepa0 = 2 days^{-1}$) allow us to obtain the experimentally observed ratio of peak TrkA to TrkA in saturating NGF when $Vdepf0$ is $0.12 days^{-1}$. The ratio of TrkA induced by 0 NGF to the TrkA induced by saturating NGF depends in addition on Vsyn0n. The value that reproduces the experimentally observed ratio is $0.038\, days^{-1}$. Using the fact that under initial conditions the average TrkA concentration increases, the

constraint $Vsyn0n - Vdepa1 \times Kddep \ll 1day^{-1}$ and assuming that the degradation rate under TrkA control is one order of magnitude larger than the TrkA independent rate, we obtain $Vdepa1 = 10/day$ and $Kd_{dep} = 0.011$. The number of surviving neurons varies roughly linearly with the total degradation rate (Equation (17) and fig. S9). Together with NGF production, the degradation rates are the main determinant of the number of neurons which will survive.

NGF

The value used for normalized in/out volume ratio of one neuron to the target tissue is $volRn = 0.04$. The rate of NGF production, $pr = 1$ is chosen such that roughly 50% of the initial $n_0 = 100$ neurons survive. NGF production has a large influence on competition (fig. S7). Reducing NGF production by a factor of two reduces the number of surviving neurons by a factor slightly larger than two, resulting in an overshoot of equilibrium.

p75

The absolute amount of p75 has little influence on the simulation, while its relative amount compared to the p75 threshold is important. Since the p75 threshold is tuned for these simulations, it is possible to fix the p75 production term. We chose $Vp75 = Kd_{p75}$ such that the production term for p75 in low TrkA is equal to the concentration of active TrkA.

The concentration of active TrkA, which leads to half-activation of p75 expression, is considered one quarter of the concentration of active TrkA which leads to half-activation of TrkA expression: $Kd_{p75} = 0.25$.

The depletion rate constants of free and active p75 are estimated at 0.5 per day: $Vdepp75f = Vdepp75a = 0.5/day$.

Apoptotic Signal

We assumed that the uptake of the apoptotic signal by sympathetic neurons has little effect on the concentration of the apoptotic signal: volRgang=0 (volume ratio of the interior of a neuron and the volume of the ganglia, normalized by the dissociation constant of the apoptotic signal from p75).

The concentration of active TrkA which leads to half-activation of apoptotic signal expression is considered the same as the concentration of active TrkA which leads to half-activation of TrkA expression: $Kd_{PUN} = 1$.

As with p75, the relative concentration of apoptotic signal to p75 threshold is more important and thus we normalize its production: $Pr_{BDNFn} = 1/n0$.

The rate constant of apoptotic signal depletion is assumed to be 1/day.

The influence of the parameters characterizing the apoptotic signal on competition is presented in fig. S10.

Influence of the Apoptotic Signal on TrkA

For $Ap_k = 5/day$, we estimated that this is the time it takes for a neuron from the

moment it receives an apoptotic signal to undergo apoptosis and die. Varying this parameter does not lead to large variations in the final neuron number.

The threshold for the active p75 receptor is chosen such that the neurons can first be susceptible to the apoptotic cue at the end of the exponential growth: $p75_{tr} = 0.01$. If the chosen threshold for protection is too high, the number of neurons which survive the competition with apoptotic signal is smaller than the number of neurons surviving the competition without apoptotic signal. If the threshold for protection chosen is too low, the competition is not hastened by addition of the apoptotic signal. There are intermediate values for which the numbers of neurons which survive the competition with apoptotic signal are similar to those which can survive the competition without it while the time it takes to reach that number is much shorter with apoptotic signal (fig. S11). For our simulations, we chose such a value: $TrkA_{tr} = 0.12$. This leads to 54% of the neurons surviving the competition with apoptotic signal while 48% of the neurons survive the competition without apoptotic signal (fig. S10).

TrkA and p75 affinities

While in the final equations for the model (25) the receptor affinities are not explicitly present, the model includes these affinities. They are implicit in equations (25) in the normalizations of $NGFn(t) = NGF(t)/Kd_{NGF}$ and $BDNFn(t) = BDNF(t)/Kd_{p75BDNF}$. It is possible to simulate the influence of dissociation constants from receptors by simultaneously changing the parameters which are normalized by them. In the case of Kd_{NGF} they are $NGFn(0)$, prn and $volRn$ (from eq 14) and for $Kd_{p75BDNF}$ they are $BDNFn(0)$, Pr_{BDNFn} and $volRgangn$ (from eq 21 and 23). These simulations are presented in fig. S16. In the absence of an apoptotic signal, if all the other parameters are constant, the affinity of NGF for TrkA has minimal influence on the number of neurons surviving the competition. This result can be intuitively understood from our assumption that most of the NGF depletion in the target tissue is a result of binding to TrkA and subsequent internalization. Thus if NGF has a lower affinity for TrkA, the equilibrium concentration in the target tissue will be higher compensating to a large extent the decrease in affinity. In the presence of apoptotic signals both affinities have ranges in which the competition progresses as presented in Fig 4. Outside of these ranges, the apoptotic signal either results in excessive neuronal death or fails to significantly speed up the competition.

REFERENCES

1. K.-F. Lee *et al.*, *Cell* **69**, 737 (1992).
2. R. Kuruvilla *et al.*, *Cell* **118**, 243 (2004).
3. C. Crowley *et al.*, *Cell* **76**, 1001 (1994).
4. C. M. Knudson, K. S. Tung, W. G. Tourtellotte, G. A. Brown, S. J. Korsmeyer, *Science* **270**, 96 (1995).
5. N. O. Glebova, D. D. Ginty, *Journal of Neuroscience* **24**, 743 (2004).
6. A. S. Mohamood *et al.*, *International Immunology* **18**, 1265 (2006).
7. R. A. Irizarry *et al.*, *Biostatistics* **4**, 249 (2003).

8. Z. Wu, R. A. Irizarry, R. Gentleman, F. Martinez Murillo, F. Spencer, *Journal of the American Statistical Association* **99**, 909 (2003).
9. B. M. Bolstad, R. A. Irizarry, M. Astrand, T. P. Speed, *Bioinformatics* **19**, 185 (2003).
10. M. A. Newton, C. M. Kendziorski, *Springer Verlag* (2003).
11. M. A. Newton, C. M. Kendziorski, C. S. Richmond, F. R. Blattner, K. W. Tsui, *Journal of Computational Biology* **8**, 37 (2001).
12. C. M. Kendziorski, M. A. Newton, H. Lan, M. N. Gould, *Statistics in Medicine* **22**, 3899 (2003).
13. R. Ihaka, R. Gentleman, *Journal of Computational Graphical Statistics* **5**, 299 (1996).
14. H. Ye, R. Kuruvilla, L. S. Zweifel, D. D. Ginty, *Neuron* **39**, 57 (2003).
15. R. Kuruvilla, H. Ye, D. D. Ginty, *Neuron* **27**, 499 (2000).
16. R. J. Pasterkamp, F. D. Winter, A. J. G. D. Holtmatt, J. Verhaagen, *Journal of Neuroscience* **18**, 9962 (1998).
17. B. E. Lonze, D. D. Ginty, *Neuron* **35**, 605 (2002).
18. X. Chen *et al.*, *Neuron* **46**, 13 (2005).
19. C. Brennan, K. Rivas-Plata, S. C. Landis, *Nature Neuroscience* **2**, 699 (1999).
20. S. X. Bamji *et al.*, *The Journal of Cell Biology* **140**, 911 (1998).
21. S. Wyatt, A. M. Davies, *The Journal of Cell Biology* **130**, 1435 (1995).
22. F. D. Miller, T. C. Mathew, J. G. Toma, *Journal of Cell Biology* **112**, 303 (1991).

Supplemental Table and Figure Legends

Table S1. List of genes whose expression is dependent on NGF in vivo.
Selected genes whose expression is down regulated in the SCG in the $NGF^{-/-};BAX^{-/-}$ mouse compared to Bax controls, and their putative functions.

Table S2. Microarray data. An Excel spreadsheet with ontologies and fold change for NGF-regulated genes identified in the described microarray analysis.

Fig. S1. RT-PCR of several candidate genes identified in the microarray screen. (**A**) Validation via RT-PCR of several microarray candidate genes that are down regulated in the $NGF^{-/-};BAX^{-/-}$ mouse Rat sympathetic neurons were grown in the presence of NGF for 2 days, deprived of NGF for 1 day, and NGF was added back for one additional day. Serial dilutions of the cDNA for these two conditions were used for RT-PCR for the indicated genes. GAPDH is used as a loading control. (**B**) In situ hybridization for TrkA using sections through the SCG from $Bax^{-/-}$ and $NGF^{-/-}$; $Bax^{-/-}$ mice. (**C**) Level of phosphorylation of TrkA and Akt in sympathetic neurons established from E18 or P3 rats and cultured for 24 hours in the presence of 30ng/mL NGF (left panels). Activity of TrkA and Akt in E18 sympathetic cultures grown for 1 DIV or 4 DIV in the presence of 30ng/mL NGF (right panels).

Fig. S2. Best fit of TrkA expression levels during development. The models used are obtained considering that the rate of TrkA expression depends on TrkA activation via a Hill function with a Hill coefficient of 1 (red) or 2 (blue). The black line is the best fit for the Hill coefficient of 1 relaxing the constraint that $TrkAani_i(t) = 1$. Data used for this analysis in part relies on data from Davies and colleagues (*21*).

Fig. S3. Fit of the model to the NGF dose-dependence of TrkA expression. The model parameters were adjusted such that the ratio of TrkA in response to 0 or a saturating amount of NGF is the same as the measured one, and the ratio of the maximal TrkA response to the TrkA response to saturating NGF is the same as the measured one. This curve is derived from 3 separate experiments in sympathetic neurons treated with the indicated concentration of NGF for 24 hours and normalized to TuJ1. The bottom panel is a representative immunoblot for this NGF dose- response curve for TrkA expression. This protein dose- response curve shows maximal TrkA levels at relatively low concentrations of NGF. At higher concentrations of NGF, TrkA levels are reduced presumably due to degradation. This may explain the difference between this protein curve and the mRNA curve presented by Davies and colleagues (*21*).

Fig. S4. Simulations of different models of competition for NGF. Row 1 (**A** to **C**) Neither TrkA synthesis nor TrkA degradation rate constant depends on NGF. Row 2 (**D** to **F**) TrkA synthesis is NGF-dependent while TrkA degradation rate constant is constant. Row 3 (**G** to **I**) TrkA synthesis is constant while TrkA degradation rate constant depends on NGF. Row 4 (**J** to **K**): Both TrkA synthesis and TrkA degradation rate constants are NGF-dependent. Column 1: (A, D, G) Rate of TrkA degradation (red) and synthesis (blue) at NGFn = 0.1, 0.3, 1 and 3. A bimodal distribution for TrkA can be obtained only if its rate of degradation and synthesis intersect at least three times, as observed in (G).

Column 2: (B, E, H) Time dependence of TrkA concentration for individual neurons. Insets focus on early TrkA accumulation. Column 3: (C, F, I) Time dependence of the average TrkA concentration, extracellular NGF concentration and number of neurons.

Fig. S5. Robustness to modifications of initial conditions. Row 1 (**A** to **C**): Initial NGF concentration 5 times lower by a factor of five. Row 2 (**D** to **F**): Initial NGF concentration 5 times as high. Row 3 (**G** to **I**): Initial TrkA concentrations 5 times lower by a factor of five. Row 4 (**J** to **K**): Initial TrkA concentration 5 times as high. In all these simulations, 48% of the neurons survive. Thus, initial values for NGF and TrkA have minimal influence on the number of neurons which will survive the competition, and only a small change in the time required for the completion of competition.

Fig. S6. Robustness to modifications of initial conditions. (Rows 1, 2 and 3) These simulations used the standard parameters values but different random seeds for the initial distribution for TrkA concentrations. For these seeds respectively 51%, 48% and 47% of the neurons survive. (Row 4) The initial number of neurons is 75. The exact distribution of TrkA concentrations has marginal influence on the number of surviving neurons. Reducing the initial number of neurons while keeping all the other parameters constant (i.e. increasing the fraction of initial neurons which could potentially survive) results in a slower competition as well as a larger number of surviving neurons (a smaller overshoot from the maximally sustainable neuron number).

Fig. S7. Robustness to modifications of parameter values regarding rates of NGF production. (**A** to **C**): NGF production reduced 50%. Final number of neurons 14. (**D** to **F**): NGF production increased 50%. Final number of neurons 92. (**G** to **I**) Volume ratio and NGF production simultaneously increased by a factor of 10. Final number of neurons unmodified at 48. (**J** to **L**): Volume ratio and NGF production simultaneously decreased by a factor of 10. Final number of neurons 49. Thus, final number of neurons depends strongly on the rate of NGF production;, however, it can be compensated by other parameters.

Fig. S8. Robustness to modifications of parameter values regrading rates of TrkA production. (**A** to **C**): NGF-dependent TrkA production reduced 10%. Final number of neurons 45. (**D** to **F**): NGF-depndent TrkA production increased 10%. Final number of neurons 52. (**G** to **I**): NGF-independent TrkA production reduced 10%. Final number of neurons 48. (**J** to **L**): NGF-independent TrkA production increased 10%. Final number of neurons 49. Hence, time course of the competition as well as the final number of neurons depends strongly on the NGF-dependent TrkA expression.

Fig. S9. Robustness to modifications of parameter values regarding TrkA depletion. (**A** to **C**): Active TrkA depletion reduced 10%. Final number of neurons 64. Note the increased time scale. (**D** to **F**): Active TrkA depletion increased 10%. Final number of neurons 41. (**G** to **I**): Free TrkA depletion reduced by a factor of 3. Final number of neurons 48. Note the increased time scale. (**J** to **L**): Free TrkA depletion increased by a factor of 3. Final number of neurons 49. Therefore, the rate constant for free TrkA depletion greatly impacts the time scale of competition while leaving the final number of neurons largely unaffected.

Fig. S10. Simulations with apoptotic signal and robustness to modifications of apoptotic signal parameters. Each neuron produces an apoptotic signal (BDNF, NT4) dependent on its amount of active TrkA. (**A** to **C**): Standard parameters; nfin = 54. (**D** to **F**): Apk reduced by a factor of 2; nfin = 43 (**G** to **I**): Apoptotic signal production and depletion decreased by a factor of 2; nfin = 54. (**J** to **L**): Apoptotic signal production and depletion increased by a factor of 2; nfin = 53.

Fig. S11. Robustness to changes in the thresholds for apoptotic and protection signals. (**A** to **C**): The threshold for active p75 is reduced by 50%; nfin = 60. (**D** to **F**): The threshold for active p75 is increased by 50%. In this case it can be observed that some neurons with low levels of TrkA escape apoptosis at early time points, but die later; nfin = 49. (**G** to **I**): Protection threshold reduced by 20%; nfin = 49. (**J** to **L**): Protection threshold increased by 20%; nfin = 44. Thus, competition was strongly dependent on parameters characterizing the thresholds for apoptosis and protection.

Fig. S12. Competition if the p75 receptor to is constitutively active. (**A** to **C**): In this simulation, the p75 receptor is considered constitutively active; its activity is 1/10th of the previous apoptotic-signal- dependent activity. The apoptotic-signal- dependent activity was neglected. (**D** to **I**): Same as (A to C); however, competition happens with two independent neuronal populations in the same ganglion. In each case, half of the neurons have access to a distinct source of NGF. The two populations of neurons and the two sources of NGF are considered identical except for the initial NGF concentrations. This simulates sympathetic neurons in one ganglion innervating of two distinct target tissues.

Fig. S13. Influence of neurons with low trophic state on the competition. Comparison of competitions without apoptotic signal in Bax null and wild- type neurons. In these simulations, we assume a neuron to be dead if its active TrkA is smaller than 0.5% of TrkA half activation of its expression (criteria much stricter than used in the other simulations). (**A** to **C**) Standard parameter values, which correspond to the Bax null control. (**D** and **E**) Simulations including an additional term for TrkA degradation corresponding to apoptosis: if normalized active TrkA is smaller than 0.02, an additional degradation with a rate constant of 10/day is added. Column 1: NGF concentration, average TrkA and neuron number. Column 2: Individual TrkA concentrations. Column 3: Histograms showing the fraction of neuron numbers with a given TrkA concentration.

Fig. S14. Influence of neurons with low trophic state on competition. Comparison of competitions with apoptotic signal in Bax null and WT neurons. Same as fig. S13 when apoptotic signal signal is present.

Fig. S15. Test of the approximation that free NGF quantity is much larger than TrkA-bound NGF. Comparison of the model using this approximation, according to equations 7 (row 1) and including the correction term as in equation 9 (row 2). The same number of neurons survive, and differences in kinetics of cell loss are marginal.

Fig. S16. Robustness to modifications of TrkA and p75 affinities.
(**A**) Time dependence of the fraction of surviving neurons in simulations without apoptotic signals for different values of the dissociation constant of NGF from TrkA varying from 20 times as large (blue) to lower by a factor of 20 (red). (**B**) The dependence on the dissociation constant of NGF from TrkA for the number of surviving neurons and the time it takes for 25% of the neurons to die . A value of 1 corresponds to the simulations used in Fig 2. (**C** and **D**) Similar to (A) and (B) for simulations in the presence of apoptotic signals. (**E** and **F**) Similar to (C) and (D) but here the dissociation constant of the apoptotic signal from p75 is varied.

Fig. S17. Expression of p75, TrkA, and P-c-Jun in P5 Bax$^{-/-}$.
(**A**) p75 expression in Bax$^{-/-}$ SCGs is localized to regions of low TrkA expression. Immunostaining for TrkA (green) and p75 (red) in P5 Bax$^{-/-}$ versus wild-type SCGs. High p75 expression in low TrkA expressing cells represents somewhat of a paradox when one considers that initial expression of p75 is at least partly dependent upon NGF. We reconcile this paradox by suggesting that final target innervation and exposure to NGF is permissive for initial p75 expression, but as trophic signaling states segregate during competition, p75 expression also segregates in an NGF- independent manner. (**B**) Double immunofluorescence for TrkA (red) and P-c-Jun (green) in SCGs from P5 Bax$^{-/-}$ and wild-type animals. Note the dramatic increase in P-c-Jun staining in Bax$^{-/-}$ compared to wild-type SCGs. P-c-Jun positive neurons are often observed to reside in close proximity to TrkA positive/P-c-Jun negative neurons. (**C**) Histogram representing the amount of TrkA staining in cells with P-c-Jun positive versus negative nuclear staining in Bax$^{-/-}$ samples from panel (B).

Fig. S18. P-c-Jun expression patterns examined in various settings.
(**A**) Immunostaining for P-c-Jun (green) and Tuj1 (red) in E18 p75$^{-/-}$ versus wild-type SCG. Note that most P-c-Jun staining is dependent on p75. (**B**) Immunostaining for P-c-Jun (green) and p75 (red) in P5 Bax$^{-/-}$ versus wild-type SCG. (**C**) Immunostaining for P-c-Jun (green) and Tuj1 (red) in P5 Bax$^{-/-}$ SCG.

Transcription

-7.75	Fos	FBJ osteosarcoma oncogene
-7.11	Hoxb5	homeo box B5
-4.33	Etv1	ets variant gene 1
-4.32	Mab21l1	mab-21-like 1 (C. elegans)
-3.49	4732477C12Rik	RIKEN cDNA 4732477C12 gene
-3.43	0710005M24Rik	RIKEN cDNA 0710005M24 gene
-2.23	Phtf1	putative homeodomain transcription factor 1
-2.13	Stat3	signal transducer and activator of transcription 3
-2.04	Mbnl2	muscleblind-like 2
-1.96	Polr2l	polymerase (RNA) II (DNA directed) polypeptide L
-1.92	Zfhx4	zinc finger homeodomain 4
-1.76	9630048M01Rik	RIKEN cDNA 9630048M01 gene
-1.76	1810023B24Rik	RIKEN cDNA 1810023B24 gene
-1.71	4933432P15Rik	RIKEN cDNA 4933432P15 gene
-1.71	Tbx3	T-box 3
-1.58	Ddef1	RIKEN cDNA 1700010G06 gene
-1.55	Smarca2	SWI/SNF related, matrix associated

Guidance/Adhesion

-5.92	Nrn1	neuritin 1
-5.5	Ntng1	netrin G1
-3.46	Cntn1	contactin 1
-3.12	Crtac1	cartilage acidic protein 1
-2.97	Cntnap2	contactin associated protein-like 2
-2.97	Chl1	cell adhesion molecule with homology to L1CAM
-2.85	Mbp	myelin basic protein
-2.7	Edil3	EGF-like repeats and discoidin I-like domains 3
-2.65	6530401D17Rik	RIKEN cDNA 6530401D17 gene
-2.62	Atrnl1	Attractin like 1
-2.54	Susd2	sushi domain containing 2
-2.34	Itga6	integrin alpha 6
-2.28	Myl1	myosin, light polypeptide 1
-2.27	Cntn3	Contactin 3
-2.24	Sema4f	sema domain, immunoglobulin domain (Ig)
-2.16	Crtac1	cartilage acidic protein 1
-2.11	6430521D13Rik	RIKEN cDNA 6430521D13 gene
-2	Nfasc	Neurofascin
-1.99	Rtn4	reticulon 4
-1.96	Flrt2	Fibronectin leucine rich transmembrane protein 2
-1.92	Pcdh9	protocadherin 9
-1.88	Plxnc1	plexin C1
-1.88	Hs6st1	heparan sulfate 6-O-sulfotransferase 1
-1.88	Anxa6	annexin A6
-1.85	Nav3	neuron navigator 3
-1.85	Pcdh10	protocadherin 10
-1.81	Caps2	calcyphosphine 2
-1.73	5730596K20Rik	RIKEN cDNA 5730596K20 gene
-1.57	Cdh4	cadherin 4
-1.5	Lsamp	limbic system-associated membrane protein

Trafficking/cytoskeleton

-3.27	Tuba4	tubulin, alpha 4
-2.87	Nefl	neurofilament, light polypeptide
-2.63	Jph4	junctophilin 4
-2.61	Coro1a	coronin, actin binding protein 1A
-2.55	Avil	advillin
-2.5	Nef3	neurofilament 3, medium
-2.5	Dncic1	dynein, cytoplasmic, intermediate chain 1
-2.3	Mbp	myelin basic protein
-2.01	Cthrc1	collagen triple helix repeat containing 1
-2.01	Myo5a	myosin Va
-1.98	Pfn2	profilin 2
-1.92	Myo1b	myosin IB
-1.87	Dmn	desmuslin
-1.77	Lrp11	low density lipoprotein receptor-related protein
-1.71	Mtap1a	microtubule-associated protein 1 A
-1.65	Col27a1	procollagen, type XXVII, alpha 1

Signaling

-14.9	Ppp1r1c	protein phosphatase 1, regulatory (inhibitor)
-4.61	Ptprg	protein tyrosine phosphatase, receptor type, G
-4.14	Akap7	A kinase (PRKA) anchor protein 7
-3.89	Pthlh	parathyroid hormone-like peptide
-3.7	Rasgrp1	RAS guanyl releasing protein 1
-3.64	Lypdc1	Ly6/Plaur domain containing 1
-3.58	Socs2	suppressor of cytokine signaling 2
-3.32	Dner	delta/notch-like EGF-related receptor
-3.12	Fgf12	fibroblast growth factor 12
-3.11	Calb1	calbindin-28K
-2.89	Dner	delta/notch-like EGF-related receptor
-2.82	Calca	calcitonin/calcitonin-related polypeptide, alpha
-2.75	Trim37	tripartite motif protein 37
-2.7	Kitl	kit ligand
-2.61	Serpini1	serine (or cysteine) proteinase inhibitor, clade I
-2.44	Rapgef5	Rap guanine nucleotide exchange factor (GEF) 5
-2.42	Camk4	calcium/calmodulin-dependent protein kinase
-2.39	Gnai1	guanine nucleotide binding alpha inhibiting 1
-2.38	F2r	coagulation factor II (thrombin) receptor
-2.32	Dab2	disabled homolog 2 (Drosophila)
-2.3	MGI:1923321	(GABA-B) receptor binding protein
-2.18	Fgf13	fibroblast growth factor 13
-2.18	Socs3	suppressor of cytokine signaling 3
-2.18	Prkcd	protein kinase C, delta
-2.1	Serpinb6a	serine (or cysteine) proteinase inhibitor, clade B
-2.07	Trim2	tripartite motif protein 2
-2.03	Olfr78	olfactory receptor 78
-2.03	Prkg1	protein kinase, cGMP-dependent, type I
-2.01	Ppp2r2b	protein phosphatase 2 (formerly 2A)
-2.01	Prkg2	Protein kinase, cGMP-dependent, type II
-2.01	Bdnf	brain derived neurotrophic factor
-1.99	4930542G03Rik	RIKEN cDNA 4930542G03 gene
-1.97	Asb1	ankyrin repeat and SOCS box- protein 1
-1.92	Dlat	dihydrolipoamide S-acetyltransferase
-1.91	Adrbk2	Adrenergic receptor kinase, beta 2
-1.91	Ppfibp2	protein tyrosine phosphatase, receptor-type
-1.87	Rhoe	ras homolog gene family, member E
-1.83	Baiap1	BAI1-associated protein 1
-1.82	Mtmr6	myotubularin related protein 6
-1.77	Rassf5	Ras association (RalGDS/AF-6) domain family 5
-1.75	Gng4	G protein, gamma 4 subunit
-1.75	Dock10	dedicator of cytokinesis 10
-1.74	Mfap3l	microfibrillar-associated protein 3-like
-1.72	Rapgef5	Rap guanine nucleotide exchange factor (GEF) 5
-1.7	Ppp1r16b	phosphatase 1, regulatory (inhibitor) 16B
-1.7	Lphn2	latrophilin 2
-1.99	Scrn1	secernin 1
-1.7	Sstr4	somatostatin receptor 4
-1.69	D5Ertd606e	DNA segment, Chr 5, ERATO Doi 606, expressed
-1.67	Dusp4	dual specificity phosphatase 4
-1.65	Dcamkl1	Double cortin, calcium dependent kinase- 1
-1.64	Ntrk1	neurotrophic tyrosine kinase, receptor, type 1
-1.63	5730522G15Rik	RIKEN cDNA 5730522G15 gene
-1.61	Ptpn3	Protein tyrosine phosphatase, type 3
-1.59	1700019B16Rik	RIKEN cDNA 1700019B16 gene
-1.56	Prkg2	protein kinase, cGMP-dependent, type II
-1.55	MGI:1920480	BMP-binding endothelial regulator
-1.51	AI790205	expressed sequence AI790205
-1.64	Ppm1l	protein phosphatase 1 (formerly 2C)-like

Synaptic

-6.1	Snca	synuclein, alpha
-2.88	Syt9	synaptotagmin 9
-2.59	Syn2	synapsin II
-2.13	Ache	acetylcholinesterase

Table 1

Metabolism

-8.13	St6galnac5	ST6-N-acetylgalactosaminide alpha-2,6-sialyltransferase 5
-7.69	Sgpp2	sphingosine-1-phosphate phosphotase 2
-3.08	Car3	carbonic anhydrase 3
-3.02	Gcnt2	glucosaminyl (N-acetyl) transferase 2, I-branching enzyme
-2.95	Ddah1	dimethylarginine dimethylaminohydrolase 1
-2.95	Idh3a	isocitrate dehydrogenase 3 (NAD+) alpha
-2.84	Ddah1	dimethylarginine dimethylaminohydrolase 1
-2.78	Grp58	glucose regulated protein
-2.76	Got1	glutamate oxaloacetate transaminase 1, soluble
-2.75	Pcsk1	proprotein convertase subtilisin/kexin type 1
-2.72	Idi1	isopentenyl-diphosphate delta isomerase
-2.53	Ass1	argininosuccinate synthetase 1
-2.49	Oxct1	3-oxoacid CoA transferase 1
-2.44	Th	tyrosine hydroxylase
-2.39	Ywhag	3-monooxgenase/tryptophan 5-monooxgenase
-2.37	Hsd17b12	hydroxysteroid (17-beta) dehydrogenase 12
-2.37	Adam19	a disintegrin and metalloproteinase domain 19 (meltrin beta)
-2.36	Idh3a	isocitrate dehydrogenase 3 (NAD+) alpha
-2.32	Acaa2	acetyl-Coenzyme A acyltransferase 2
-2.32	Oxct1	3-oxoacid CoA transferase 1
-2.3	Ptgds	prostaglandin D2 synthase (brain)
-2.28	MGI:1919030	myo-inositol 1-phosphate synthase A1
-2.28	Fdps	farnesyl diphosphate synthetase
-2.27	Eno2	enolase 2, gamma neuronal
-2.24	Mrpl16	mitochondrial ribosomal protein L16
-2.23	Asl	argininosuccinate lyase
-2.17	Rps6ka2	ribosomal protein S6 kinase, polypeptide 2
-2.17	Fstl5	follistatin-like 5
-2.17	Fbxo2	F-box only protein 2
-2.15	Car3	carbonic anhydrase 3
-2.14	Acsl4	acyl-CoA synthetase long-chain family member 4
-2.14	Acdc	adipocyte, C1Q and collagen domain containing
-2.1	Aldoa	aldolase 1, A isoform
-2.09	Ckb	creatine kinase, brain
-2.09	Hmgcs1	3-hydroxy-3-methylglutaryl-Coenzyme A synthase 1
-2.08	MGI:1917275	brain acyl-CoA hydrolase
-2.07	Acadl	acetyl-Coenzyme A dehydrogenase, long-chain
-2.06	Sult4a1	sulfotransferase family 4A, member 1
-2.05	C920006C10Rik	RIKEN cDNA C920006C10 gene
-2.04	2700017M01Rik	RIKEN cDNA 2700017M01 gene
-2.02	Cycs	cytochrome c, somatic
-2.01	2810457I06Rik	RIKEN cDNA 2810457I06 gene
-2	Cs	citrate synthase
-1.99	Hmgcs1	3-hydroxy-3-methylglutaryl-Coenzyme A synthase 1
-1.99	Aco2	aconitase 2, mitochondrial
-1.99	Gpi1	glucose phosphate isomerase 1
-1.98	Hsd17b12	hydroxysteroid (17-beta) dehydrogenase 12
-1.98	Aldoa	aldolase 1, A isoform
-1.98	4921517B04Rik /// LO	similar to FLJ23033 protein
-1.98	Aldoa	aldolase 1, A isoform
-1.97	Dgkh	Diacylglycerol kinase, eta
-1.92	Bpnt1	bisphosphate 3'-nucleotidase 1
-1.91	LOC14433 /// LOC38	GAPDH
-1.91	Acsl1	Acyl-CoA synthetase long-chain family member 1
-1.9	Aldoc	aldolase 3, C isoform
-1.89	Asph	aspartate-beta-hydroxylase
-1.88	Pygl	liver glycogen phosphorylase
-1.86	Aacs	acetoacetyl-CoA synthetase
-1.85	Pde4b	phosphodiesterase 4B, cAMP specific
-1.85	Coasy	Coenzyme A synthase
-1.84	Mppe1	Metallophosphoesterase 1
-1.83	Bckdhb	branched chain ketoacid dehydrogenase E1,
-1.82	Bdh	3-hydroxybutyrate dehydrogenase (heart, mitochondrial)
-1.82	Clgn	calmegin

Channel/transporter

-10	Htr3a	5-hydroxytryptamine (serotonin) receptor 3A
-8.09	Atp1a1	ATPase, Na+/K+ transporting, alpha 1 polypeptide
-6.69	Slc17a6	sodium-dependent inorganic phosphate cotransporter
-5.98	Atp7a	ATPase, Cu++ transporting, alpha polypeptide
-4.07	Scn11a	sodium channel, voltage-gated, type XI, alpha polypeptide
-3.52	Atp8a1	ATPase, aminophospholipid transporter (APLT)
-3.21	Htr3b	5-hydroxytryptamine (serotonin) receptor 3B
-2.62	Scn7a	sodium channel, voltage-gated, type VI, alpha polypeptide
-2.43	Atp1b1	ATPase, Na+/K+ transporting, beta 1 polypeptide
-2.42	Fxyd7	FXYD domain-containing ion transport regulator 7
-2.33	Atp9a	ATPase, class II, type 9A
-2.19	Trpa1	transient receptor potential cation channel
-2.18	Sec61a2	Sec61, alpha subunit 2 (S. cerevisiae)
-2.14	Slc31a1	solute carrier family 31, member 1
-2.14	P2rx2	purinergic receptor P2X, ligand-gated ion channel, 2
-2.13	Slc6a2	neurotransmitter transporter, noradrenalin, member 2
-2.12	Slc6a17	neurotransmitter transporter), member 17
-2.1	Synpr	synaptoporin
-2.02	Fabp4	fatty acid binding protein 4, adipocyte
-2.02	Grik1	Glutamate receptor, ionotropic, kainate 1
-1.98	Edg3	sphingolipid G-protein-coupled receptor, 3
-1.96	Atp6v1b2	ATPase, H+ transporting, V1 subunit B, isoform 2
-1.9	Slc35a2	UDP-galactose transporter, member 2
-1.88	Slc15a2	H+/peptide transporter, member 2
-1.86	Trappc4	trafficking protein particle complex 4
-1.83	Slc25a1	mitochondrial carrier, citrate transporter, member 1
-1.81	Nrxn1	neurexin I
-1.76	Sfxn5	sideroflexin 5
-1.74	A230052E19Rik	RIKEN cDNA A230052E19 gene

Survival

-9.68	Hspa1b /// Hspa1a	heat shock protein 1B /// heat shock protein 1A
-1.99	Bcl2	B-cell leukemia/lymphoma 2

Other

-8.91	Cyr61	cysteine rich protein 61
-3.25	Hspa4	heat shock protein 4
-3.08	Tm7sf2	transmembrane 7 superfamily member 2
-2.33	Fkbp1a	FK506 binding protein 1a
-2.16	Prx	periaxin
-2.07	Olfm3	olfactomedin 3
-2.04	Hsp105	heat shock protein 105
-2	2300002D11Rik	RIKEN cDNA 2300002D11 gene
-1.94	Hspb8	heat shock 27kDa protein 8
-1.68	Huwe1	HECT, UBA and WWE domain containing 1
-1.61	Eif5a2	eukaryotic translation initiation factor 5A2

Table 1-cont.

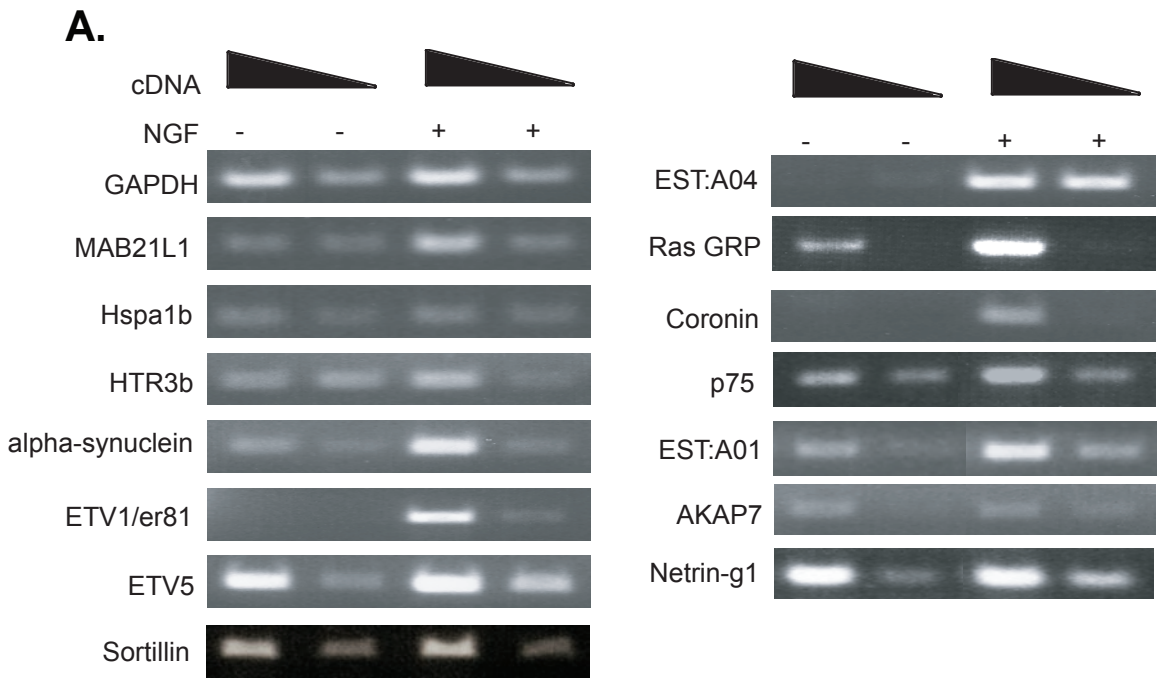

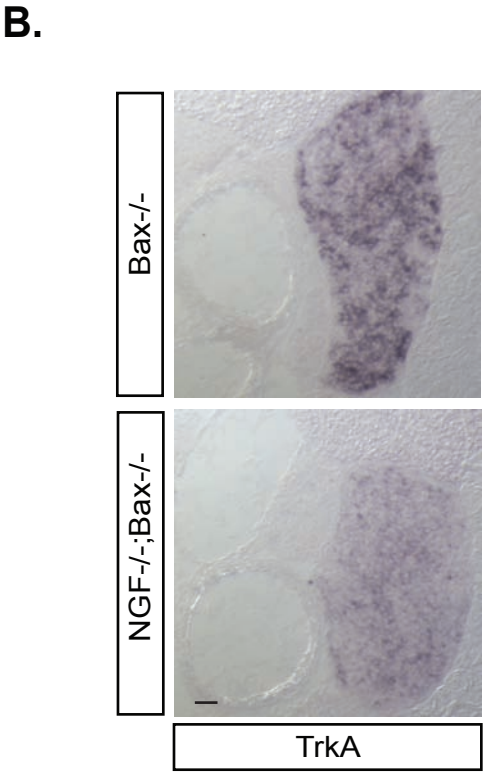

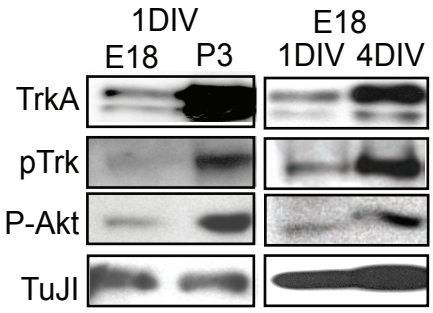

Supplemental Figure 1

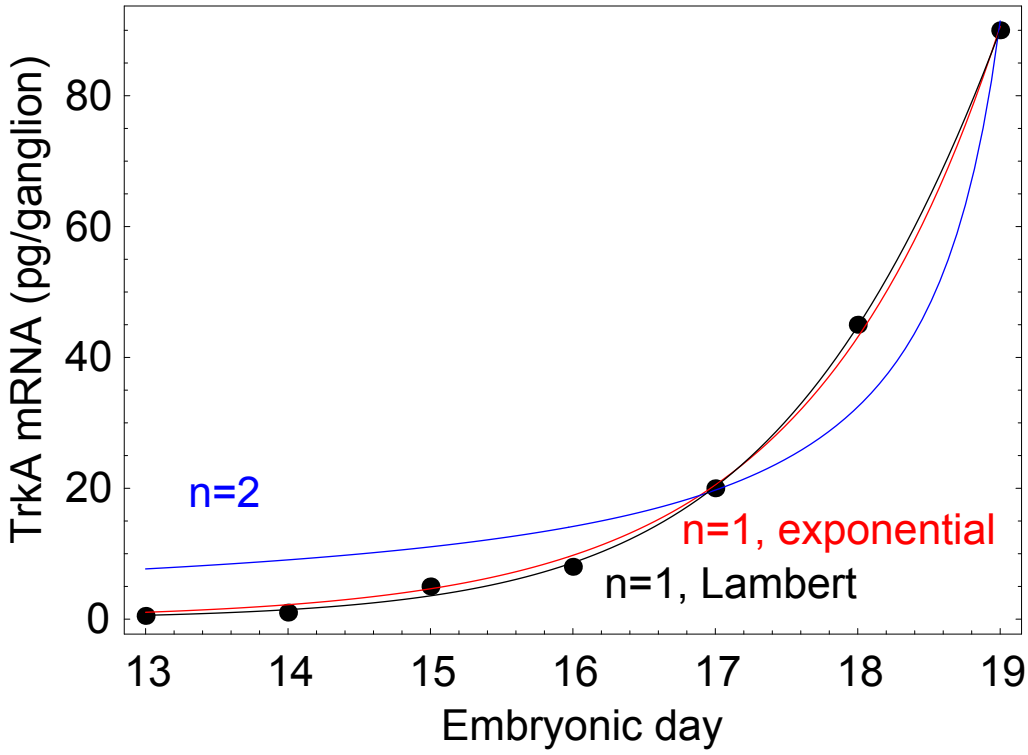

Supplemental Figure 2

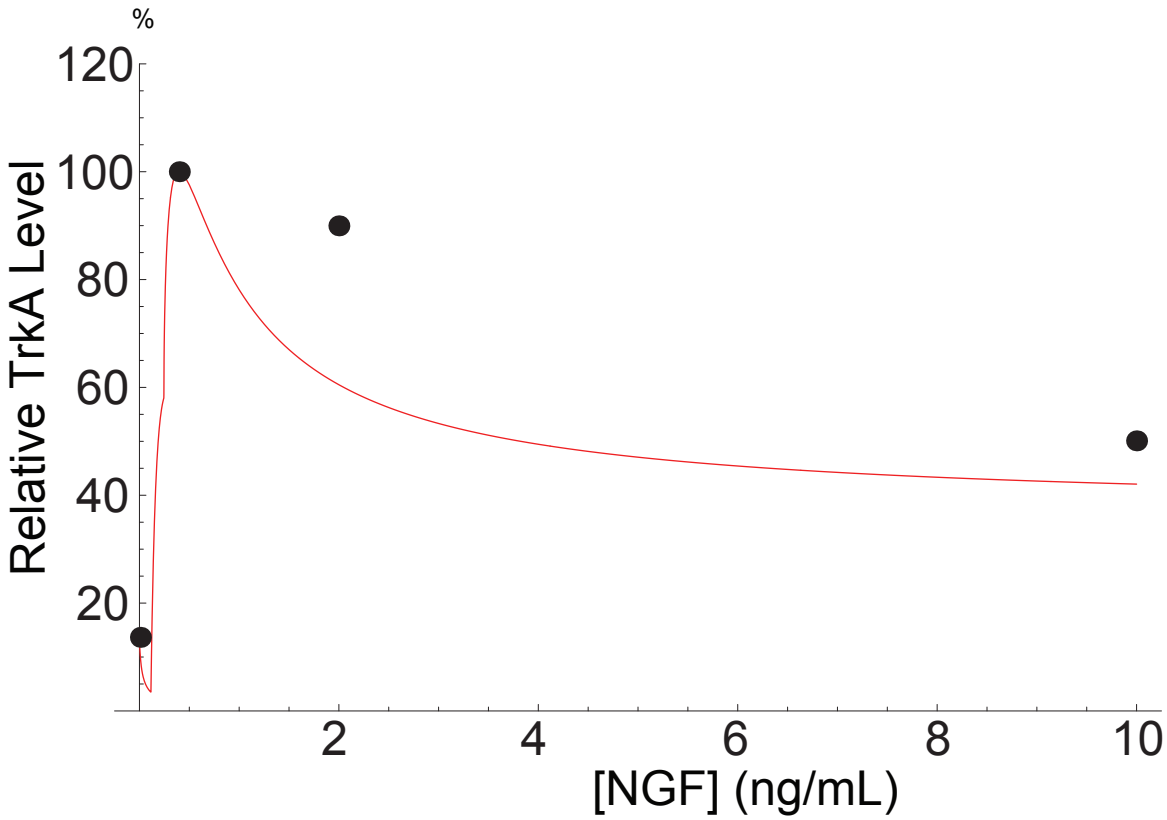

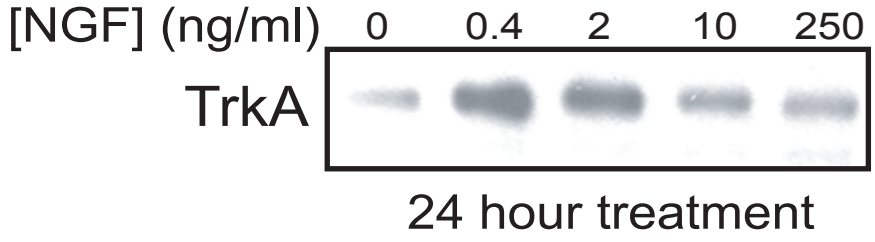

Supplemental Figure 3

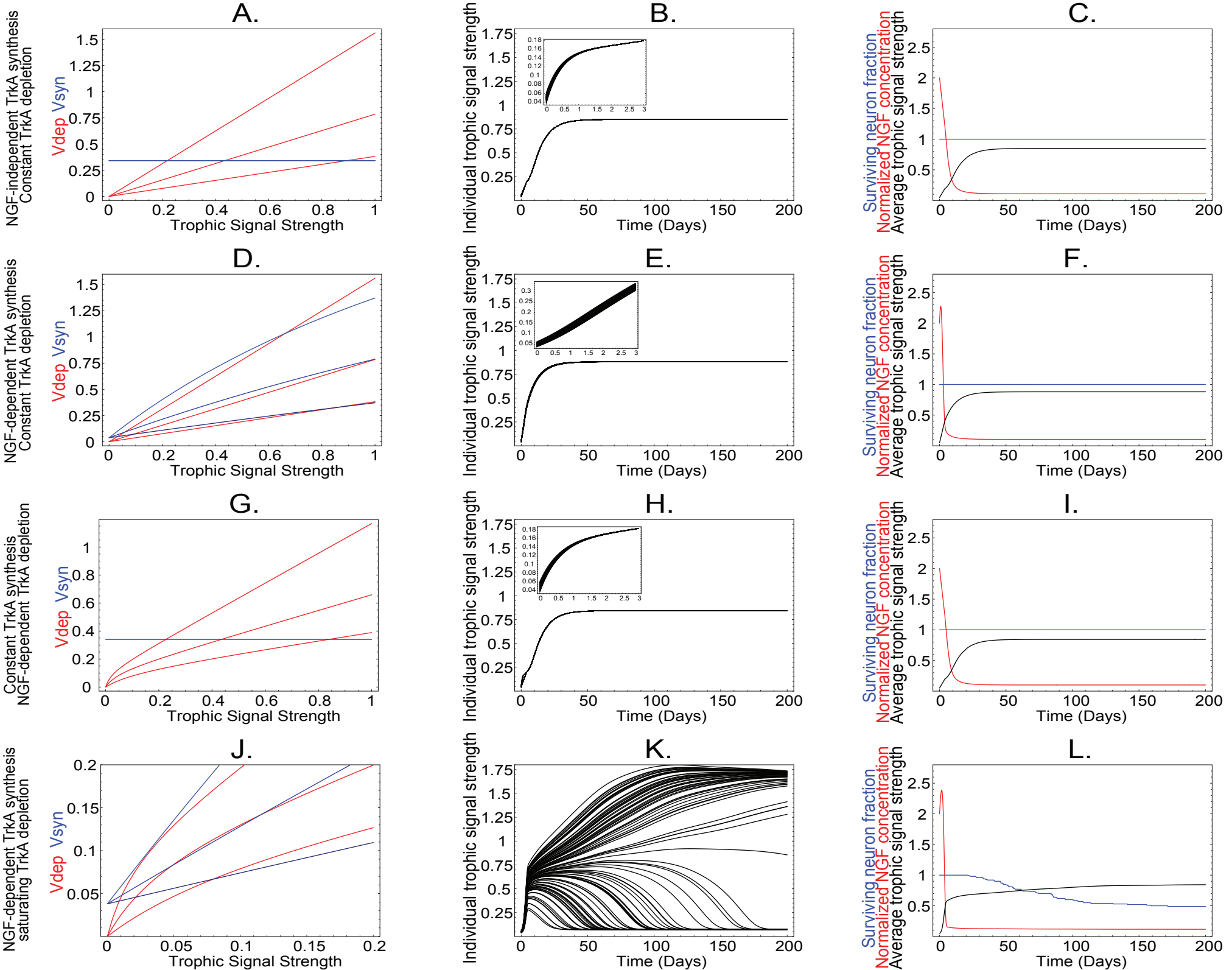

Supplemental Figure 4

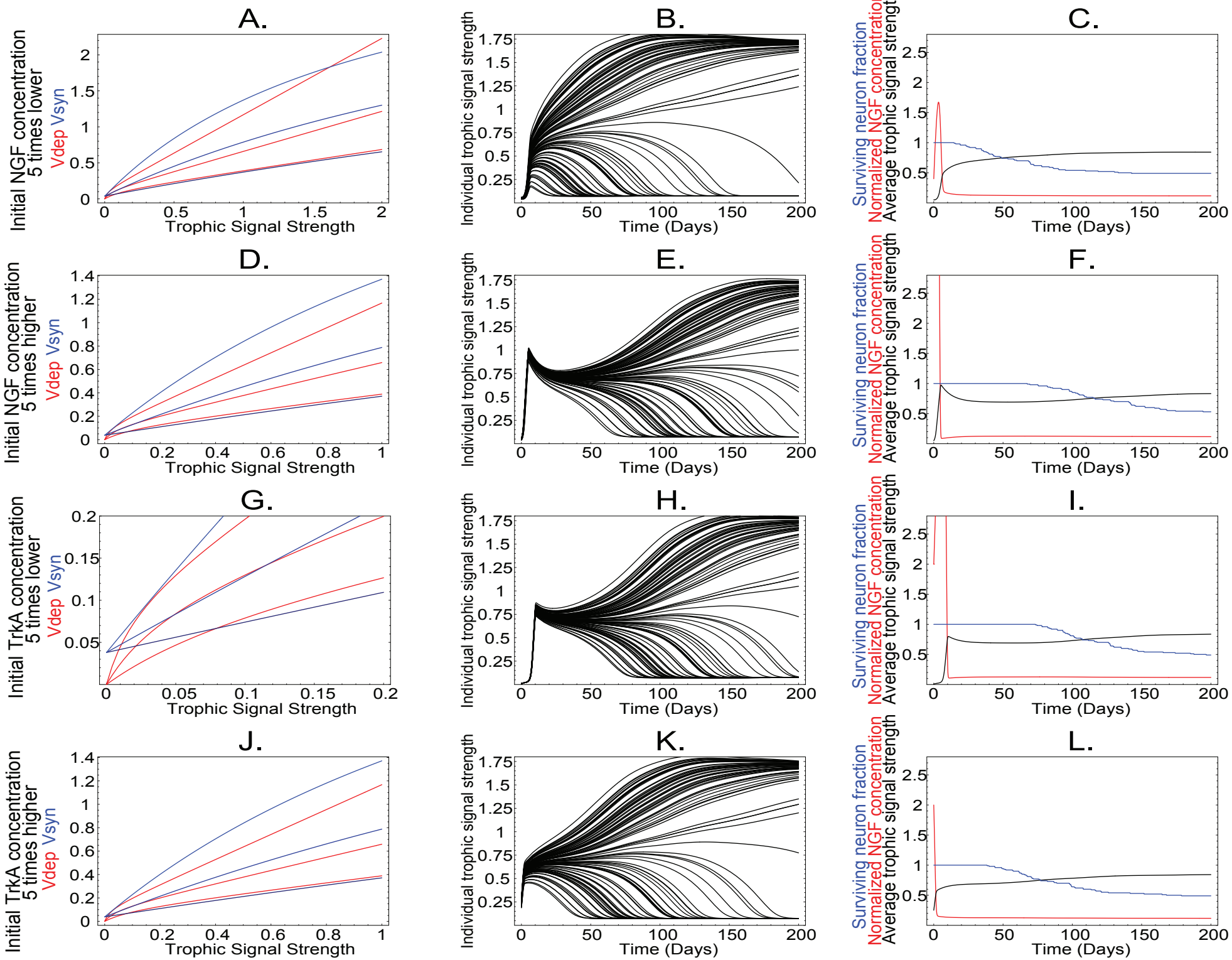

Supplemental Figure 5

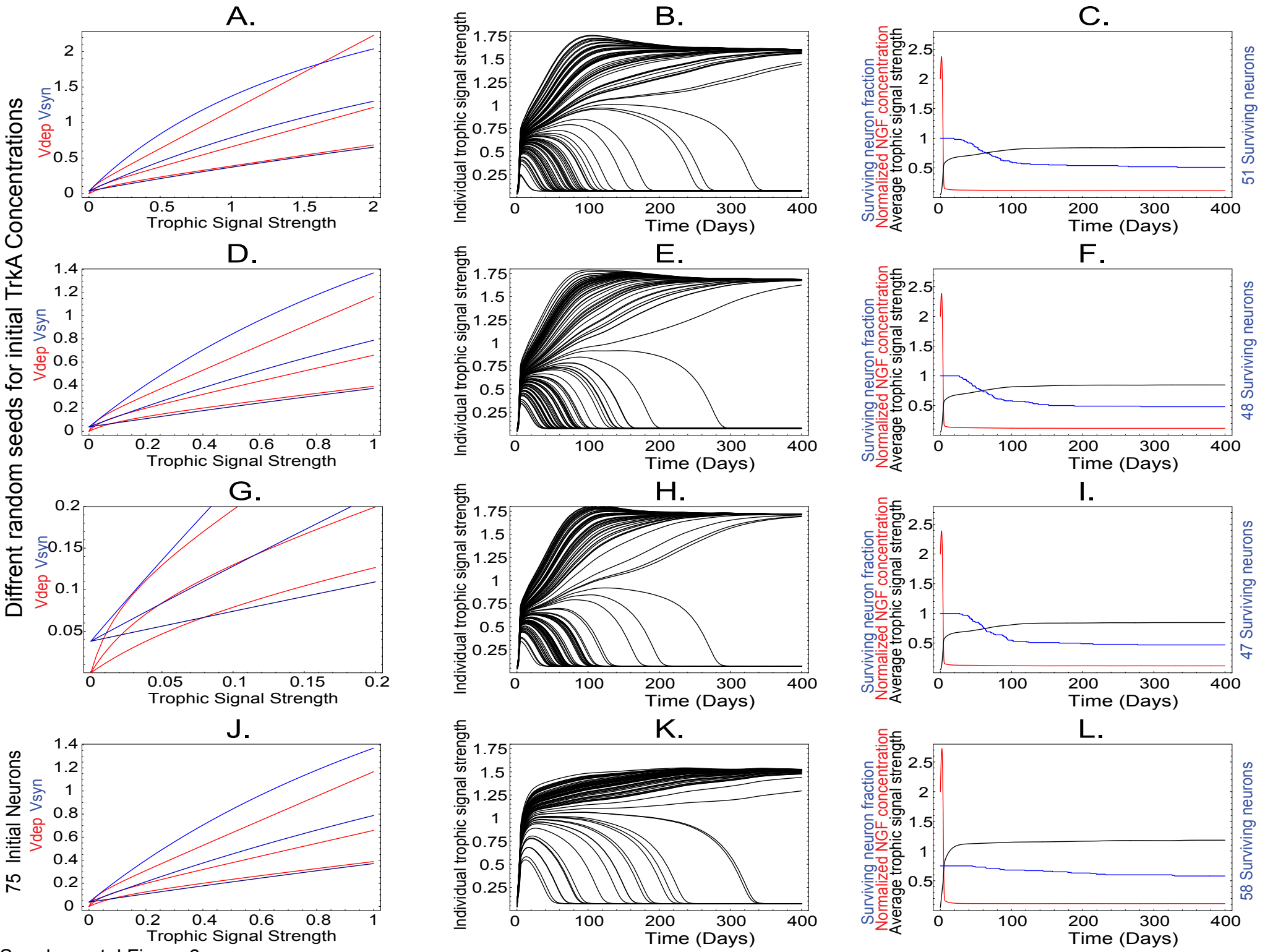

Supplemental Figure 6

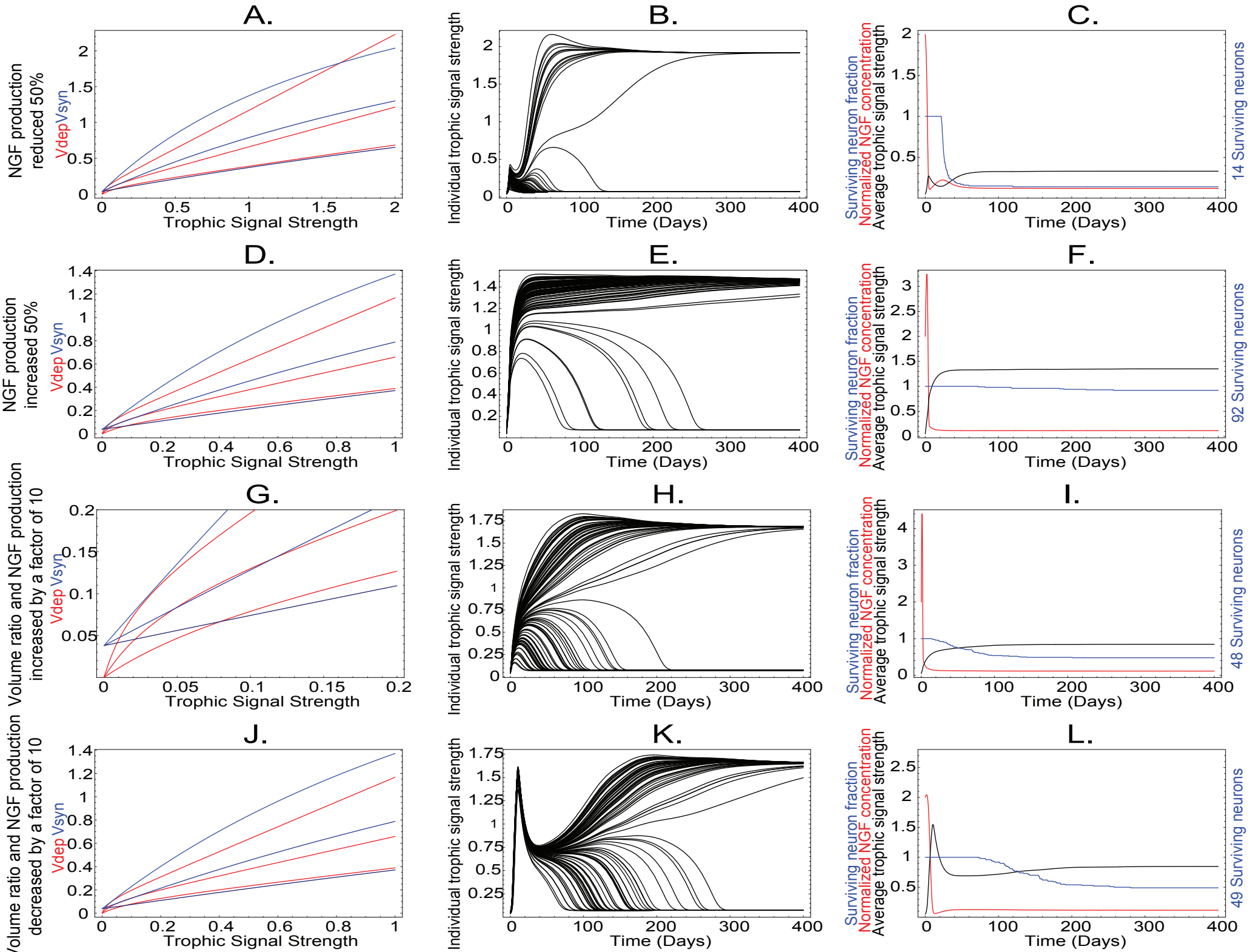

Supplemental Figure 7

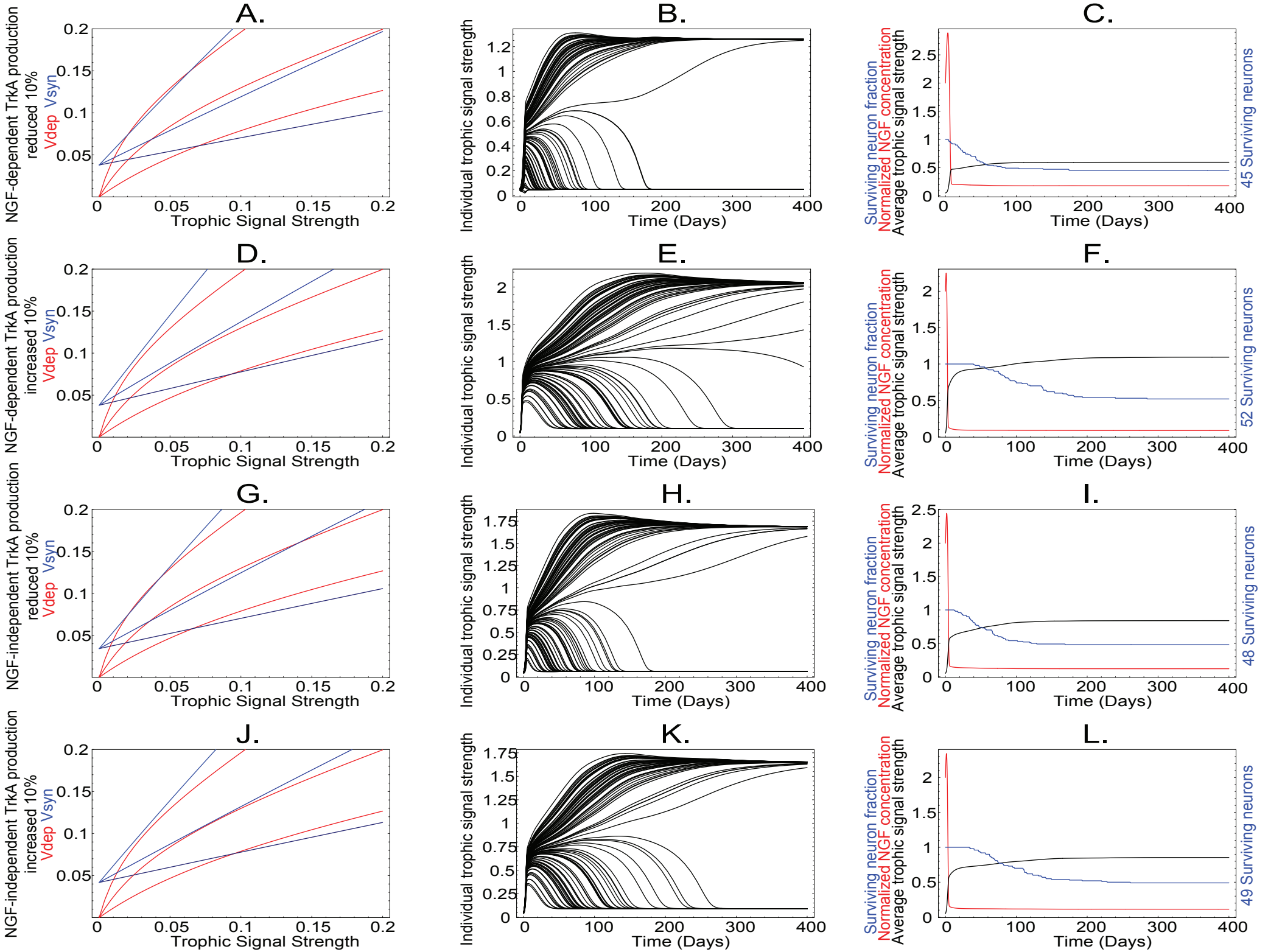

Supplemental Figure 8

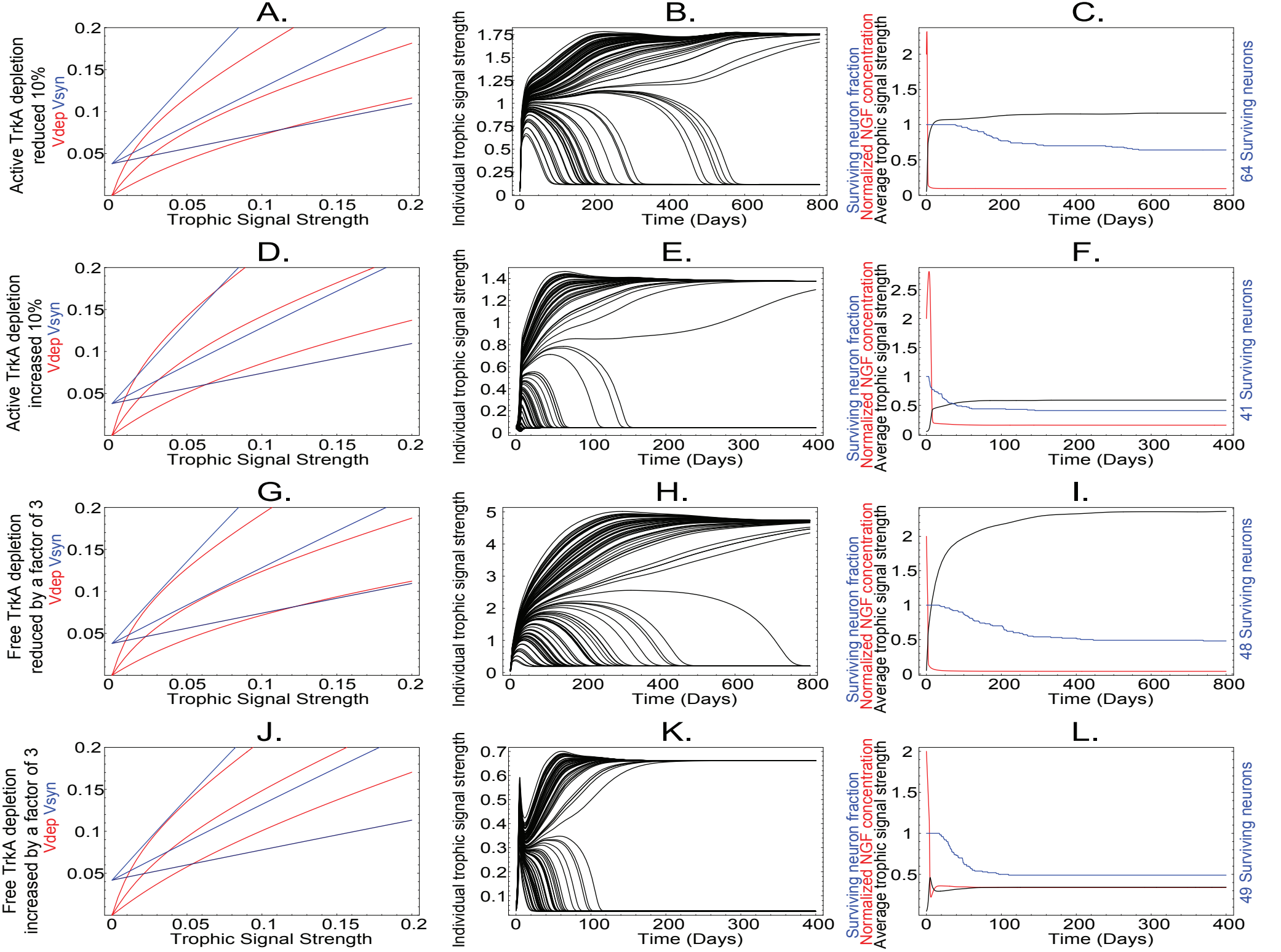

Supplemental Figure 9

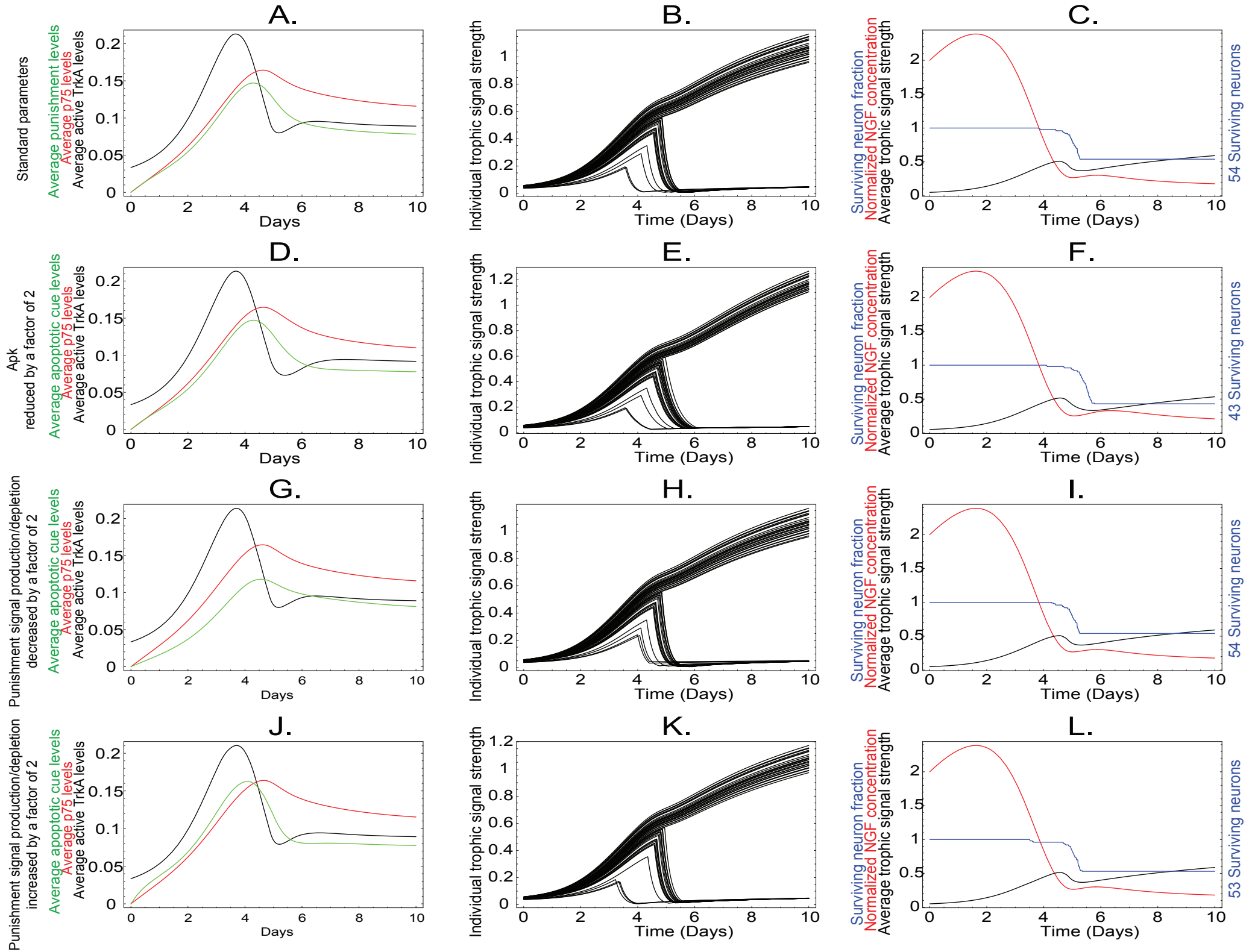

Supplemental Figure 10

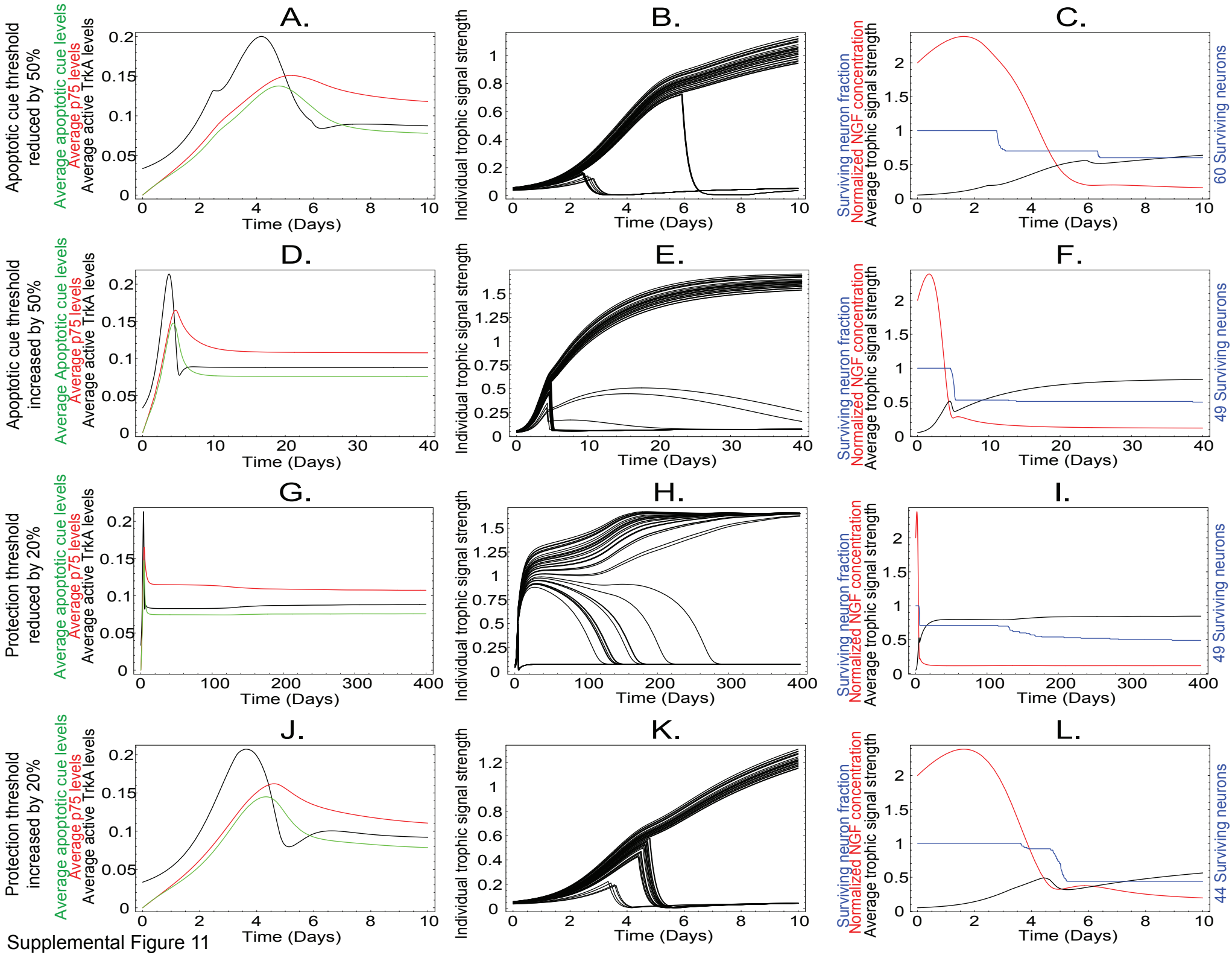

Supplemental Figure 11

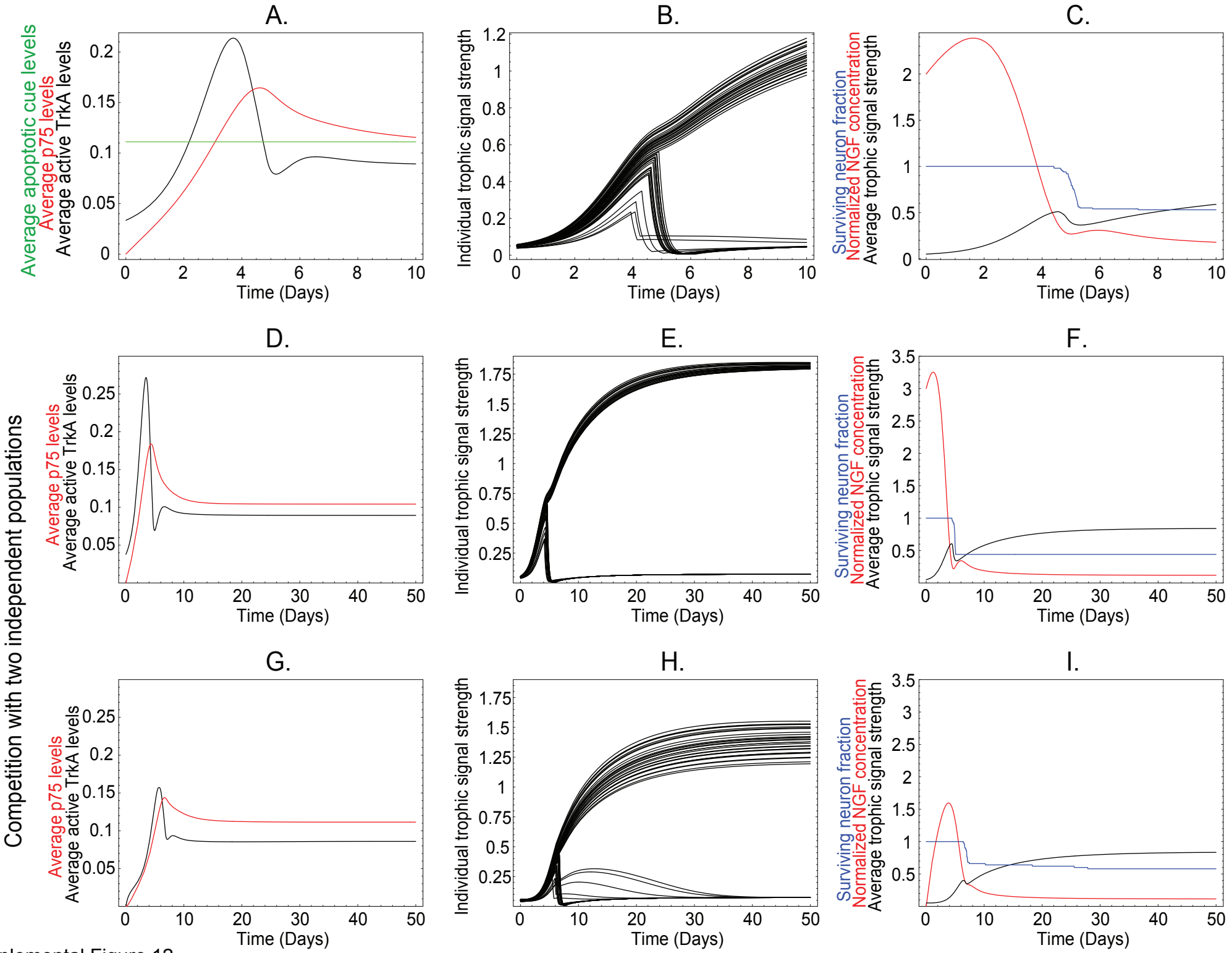

Supplemental Figure 12

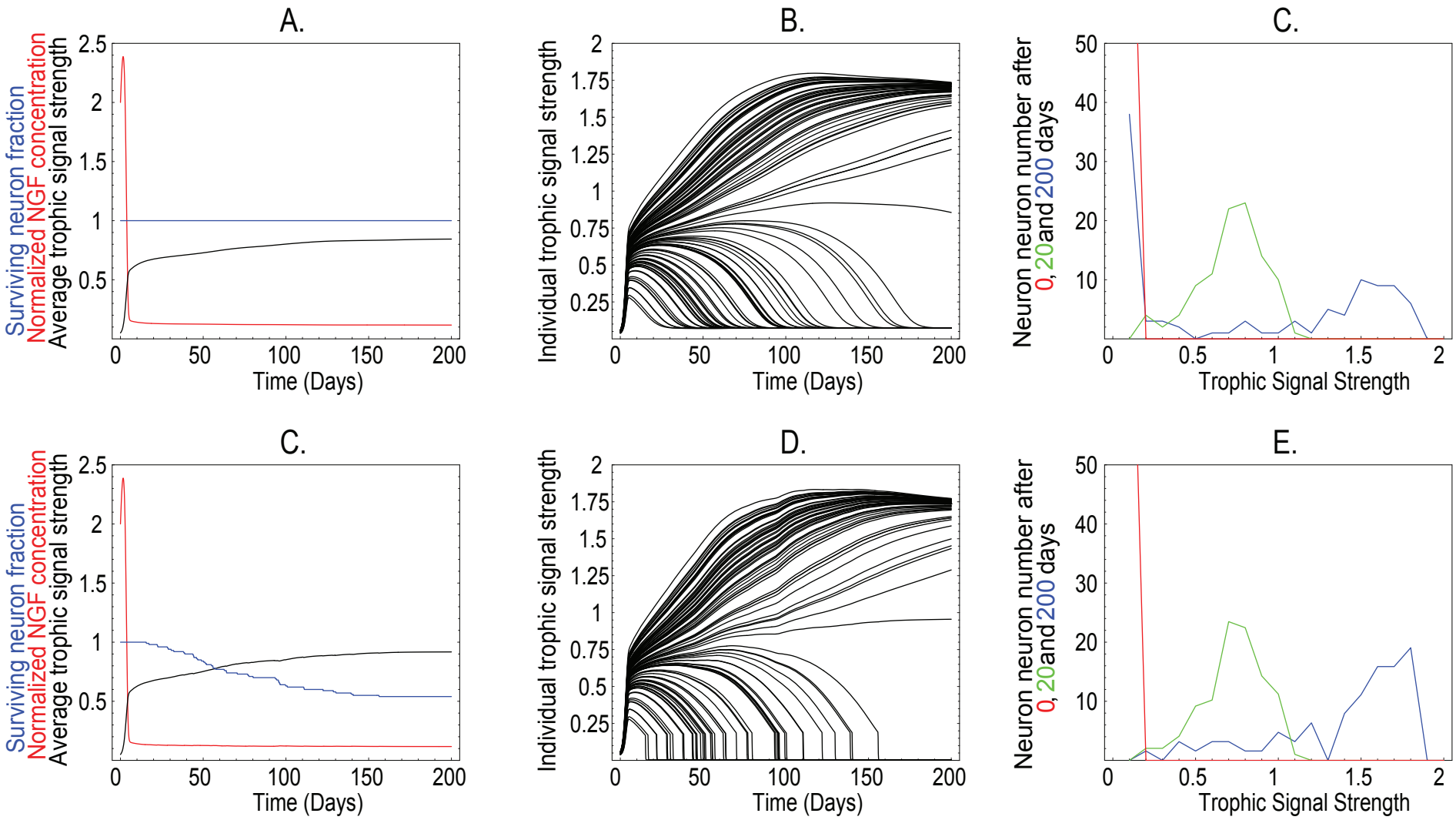

Supplemental Figure 13

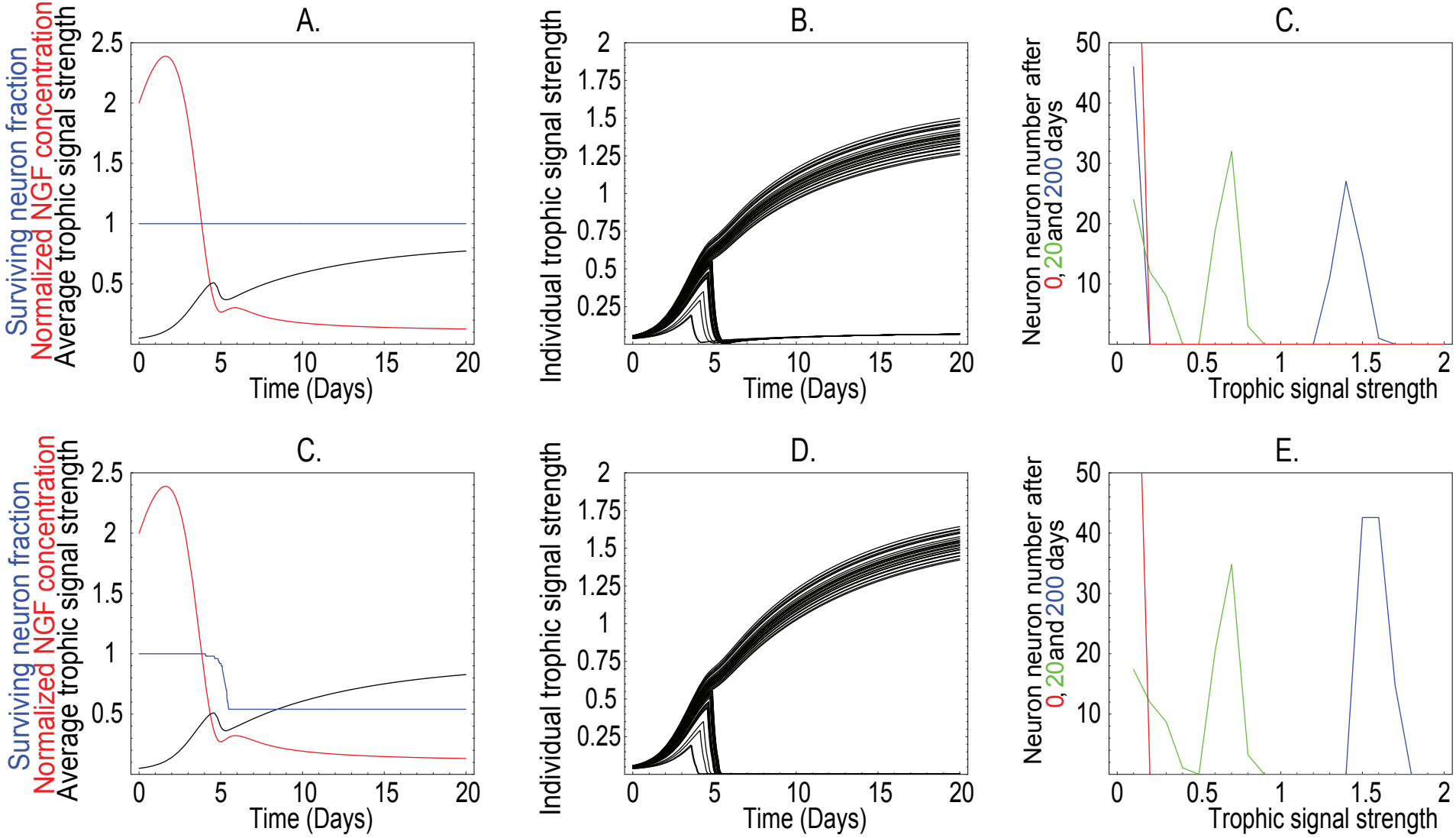

Supplemental Figure 14

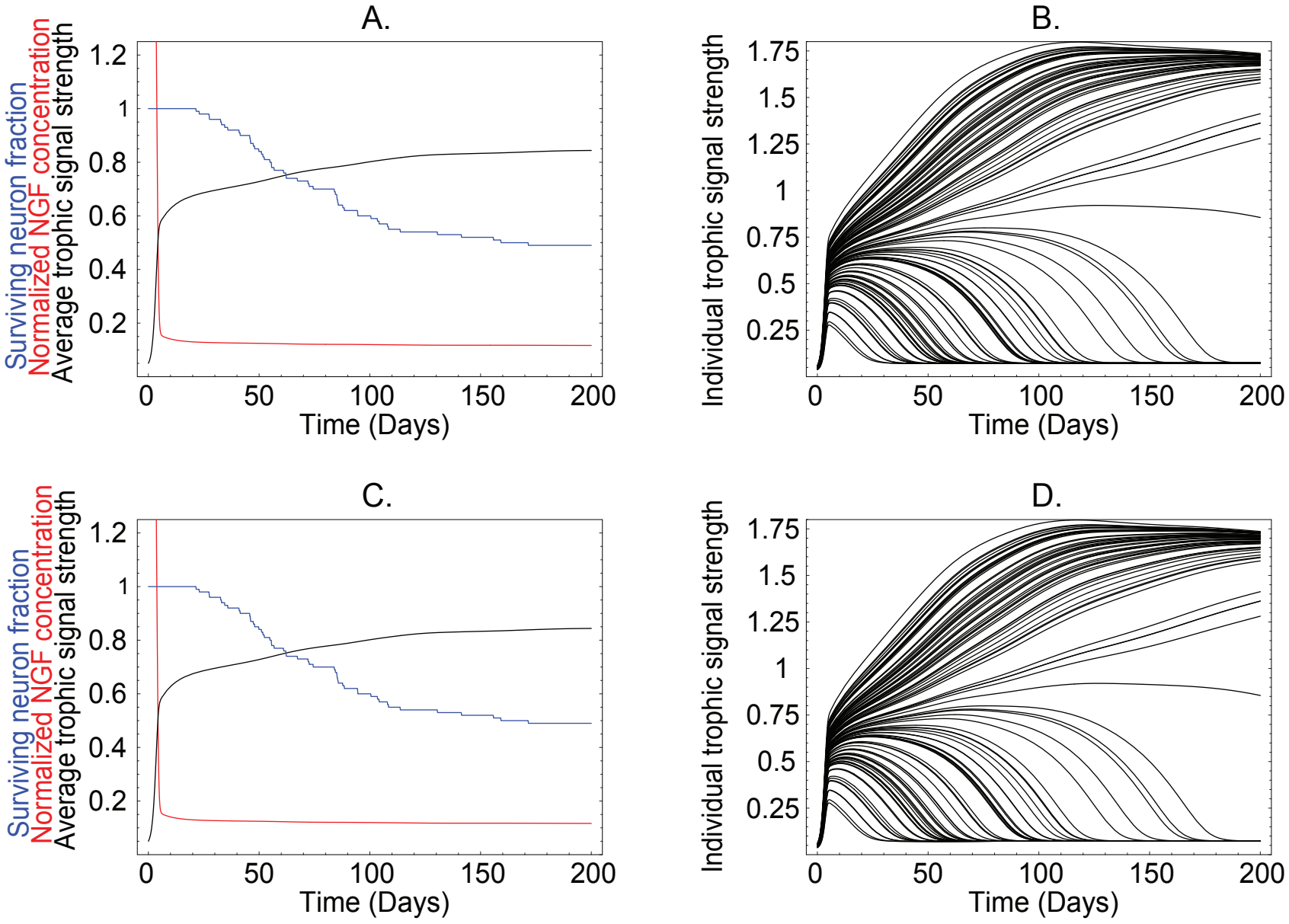

Supplemental Figure 15

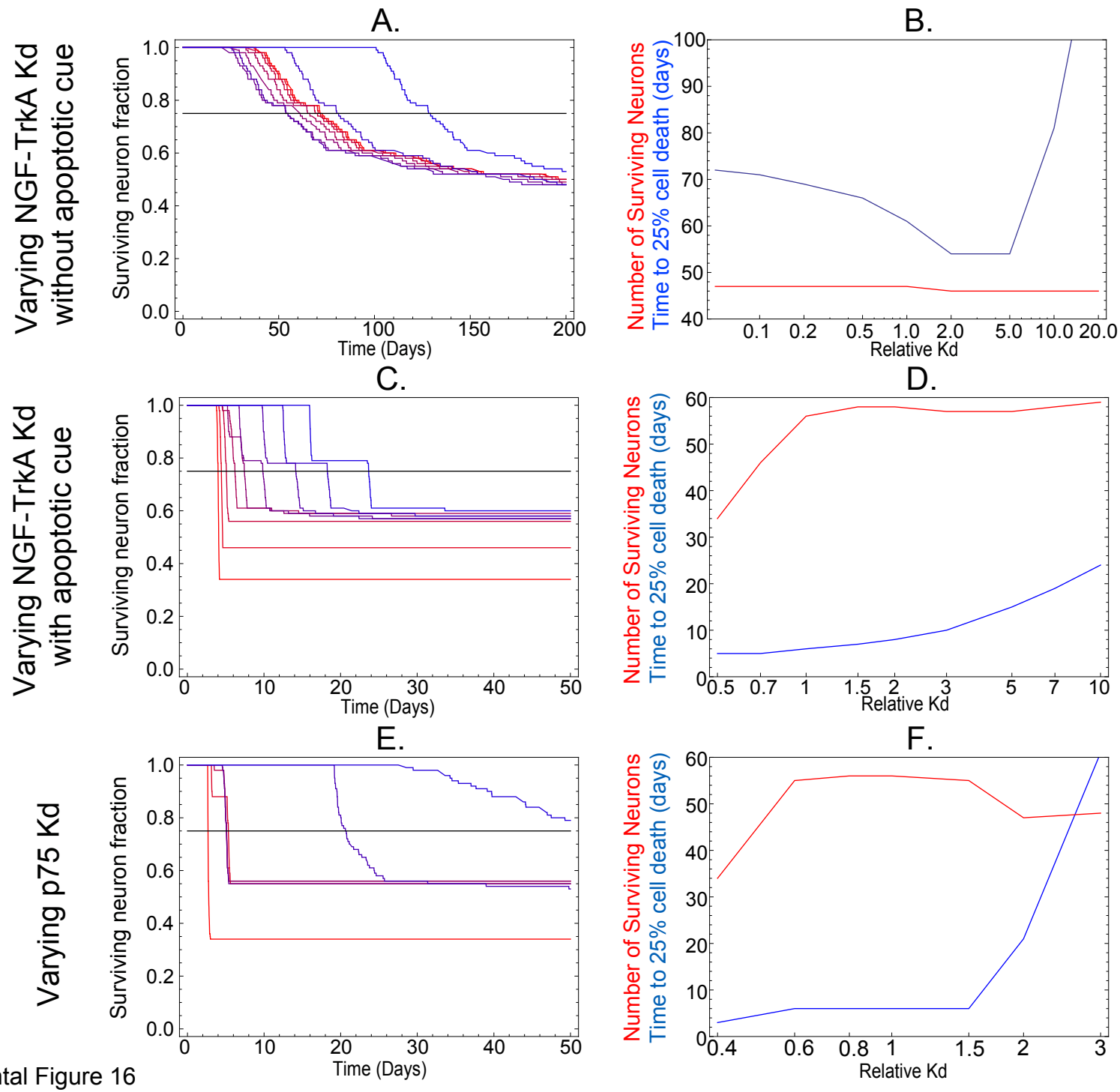

Supplemental Figure 16

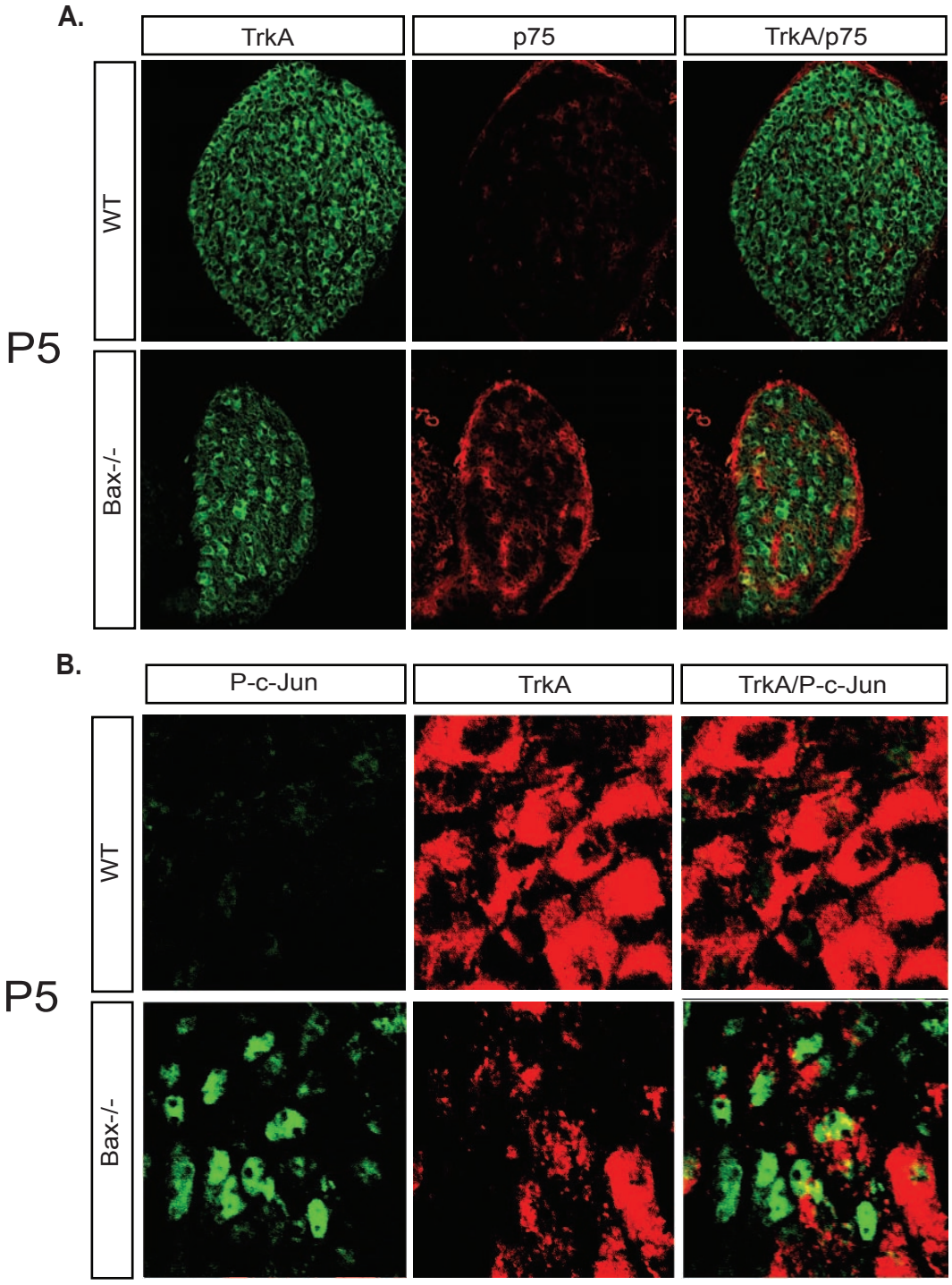

Supplemental Figure 17

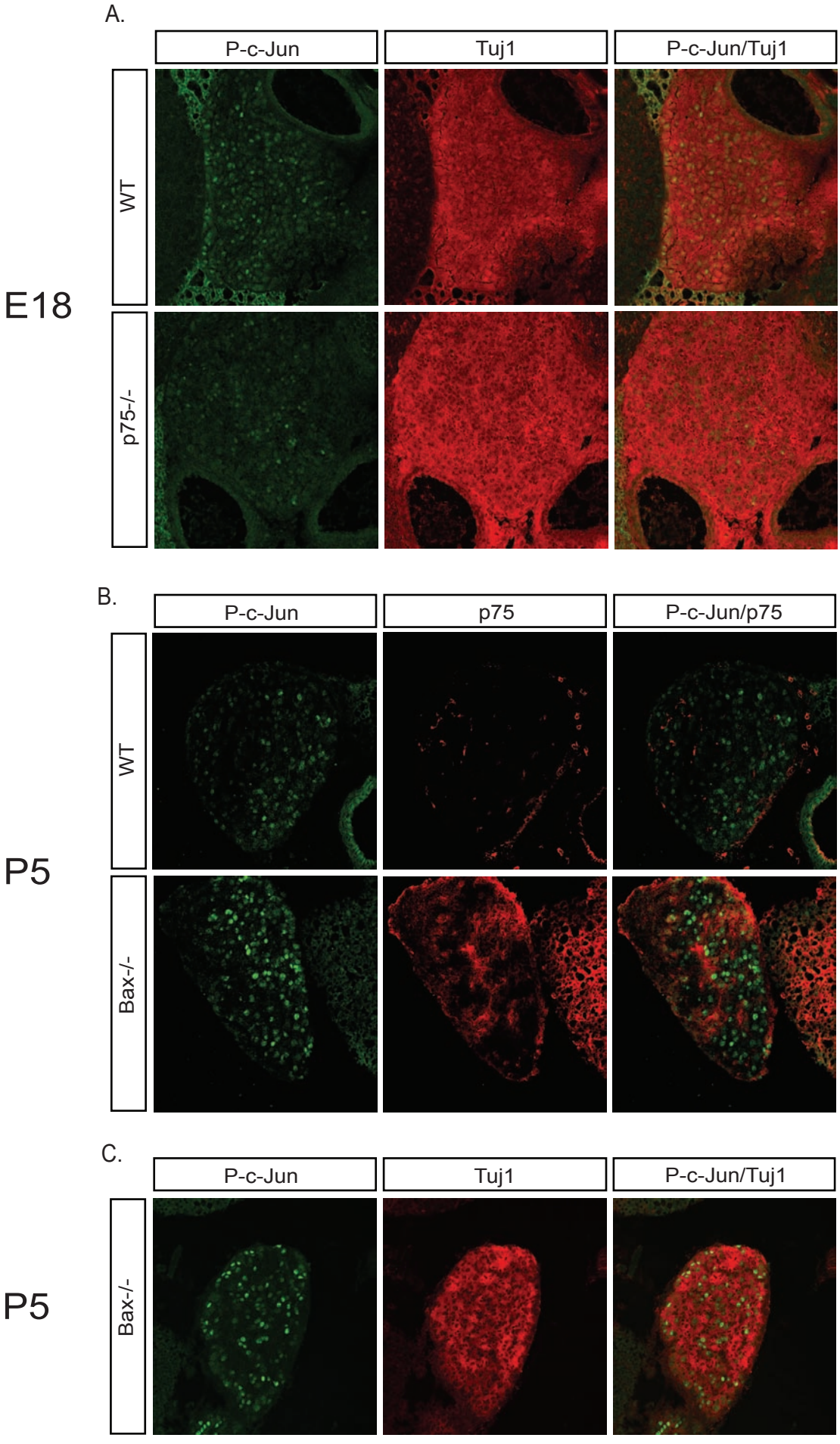

Supplemental Figure 18